

# 16

## Foams in Glass Manufacturing

*Laurent Pilon*

### 16.1 Introduction

The glass manufacturing industry provides products critical to a wide range of applications, including (i) container glass for consumer products, (ii) flat glass for automotive and buildings, (iii) fiberglass for thermal insulation, roofing, and reinforced composite materials, and (iv) specialty glass such as liquid crystal displays, optical communication, and lighting, to name a few [1]. Container glass represents more than 65% of the mass of glass produced worldwide [2]. In 2009, the US glass industry produced about 20 millions tons of glass or 20% of the global production and employed about 91,000 people for industry revenues of \$21.6 billion [3]. During the past two decades, business competition and economic challenges have forced glass manufacturers worldwide to increase productivity and product quality. They have also faced ever more stringent regulations for combustion-generated pollutant emissions.

Soda-lime-silica glass, also known as soda-lime glass, is the most common type of glass used for containers, lighting devices, and windows for buildings and automotive applications [4, 5]. It typically contains 60–75 wt%  $\text{SiO}_2$ , 12–18 wt%  $\text{Na}_2\text{O}$ , and 5–12 wt%  $\text{CaO}$ . Borosilicate glass is another common type of glass used for its chemical durability and its low thermal expansion coefficient as glassware in the chemical industry and laboratories, as flat panel display, and as cookware [4]. Their typical composition contains 70–80 wt%  $\text{SiO}_2$ , 7–13 wt%  $\text{B}_2\text{O}_3$ , 4–8 wt%  $\text{Na}_2\text{O}$  and  $\text{K}_2\text{O}$ , and 2–7 wt%  $\text{Al}_2\text{O}_3$  [4]. In addition, E-glasses are used in fiberglass for thermal and acoustic insulation for buildings as well as for textile and reinforced plastics. They are aluminosilicate glass with typical composition of 52–6 wt%

$\text{SiO}_2$ , 16–25 wt%  $\text{CaO}$ , 12–16 wt%  $\text{Al}_2\text{O}_3$ , 5–13 wt%  $\text{B}_2\text{O}_3$  and 1 wt%  $\text{Na}_2\text{O}$  and  $\text{K}_2\text{O}$  [6,7]. Finally, vitreous silica is made only of  $\text{SiO}_2$  and used for optical fiber, optical components, and in high temperature applications due to its large melting temperature [8].

The cost and quality of nearly all commercial glass products, as well as pollutant emissions associated with their production, are determined by the performance of the glass melting and delivery systems. Their performance depends, for a large part, on efficient heat transfer from the hot combustion space to the raw materials and to the glassmelt [9]. Heat transfer by thermal radiation accounts for the major fraction of the energy required for the fusion and melting of the raw materials [10].

Unfortunately, for numerous reasons discussed in this chapter, glass foam typically covers at least one-third of the molten glass surface [11]. Bubbles contained in the foam act as a collection of scatterers that reflect and backscatter part of the incident radiation coming from the combustion space [12–17]. Therefore, glass foam constitutes a major resistance to radiative heat transfer from the combustion space to the raw material and to the glassmelt [12, 13]. This, in turn, negatively affects the glass quality, energy efficiency, pollutant emission, and furnace lifetime [18].

### 16.1.1 The Glass Melting Process

Figure 16.1 shows a flow diagram of the glass manufacturing process from the mixing and conditioning of the raw material to the final glass product. The so-called batch is the raw material consisting of silica sand, sodium carbonate (soda ash), calcium carbonate (lime), cullets (broken glass), and various compounds including potassium carbonate (potash), boron compounds, nitrates, alumina, stabilizer, and coloring agents depending on the desired final glass composition [4, 19]. Refining agents are also added to the batch to help remove small gas bubbles. The batch is melted and the resulting molten glass is refined to remove potential bubbles and ensure homogenization, i.e., the dissolution and uniform distribution of all components [4, 20]. The refined glass then flows to the forehearth where it is conditioned before being formed and annealed into the final glass products. The forehearth consists of a cooling and a conditioning zone. The cooling zone ensures controlled cooling and uniform temperature of the molten glass, while the conditioning zone reheats and sometimes stirs the glassmelt.

Glass melting tanks commonly used in the glass industry include combustion-type furnaces and cold-top electric melters [2, 21, 22]. They represent a major capital investment. Combustion-type furnaces feature a waist or a submerged throat connecting the melting to the conditioning regions [23]. For example, float glass furnaces are often waist-type and cross-fired regenerative furnaces [1, 24]. The bottom of the tank is often stepped [24]. This type of furnace is fairly large and used to produce large quantity of glass products (100–1000 tons/day) such as flat glass sheets [4]. Submerged throat furnaces are used, for example, to produce glassware, TV panels, and container glass [1]. They consist of a melting tank and a refiner (or working end) connected by a channel also called a throat. Figure 16.2 shows a schematic of a typical submerged throat glass melting tank consisting of the combustion space, the glassmelt, and the refractory walls including the ceiling of the furnace called the crown.

The combustion space features large turbulent flames providing thermal energy necessary to melt the glass batch and to refine the molten glass. Combustion-type furnaces may differ in terms of (i) fuel (e.g., natural gas or pulverized coal), (ii) oxidizer (air or commercial

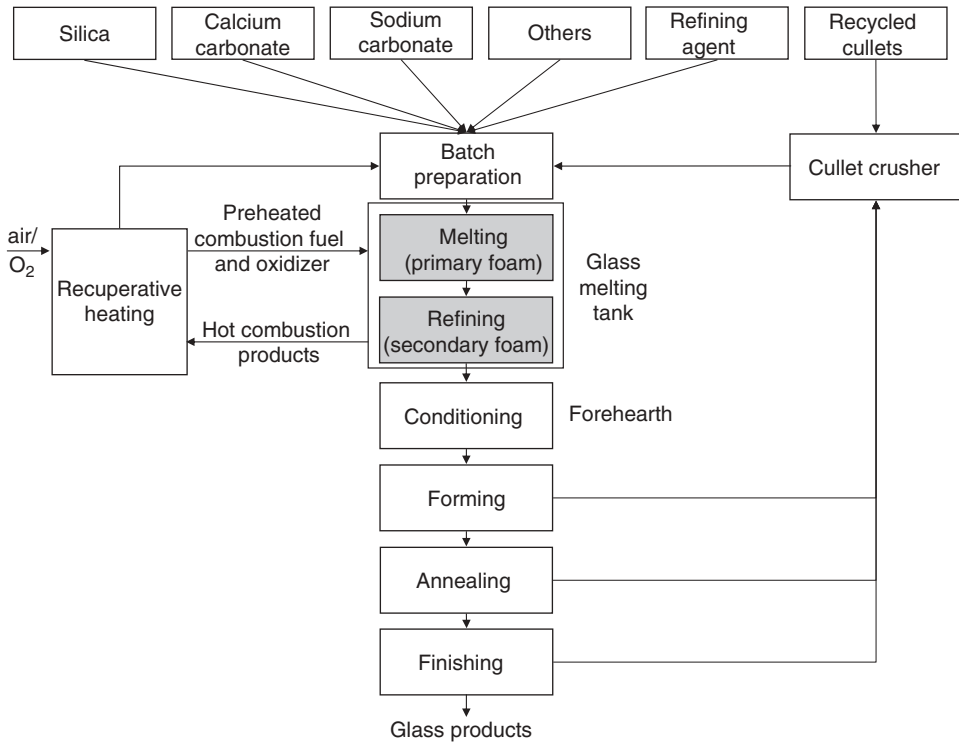


**Fig. 16.1** Diagram of the glass manufacturing process. Grey boxes indicate where glass foams are observed.

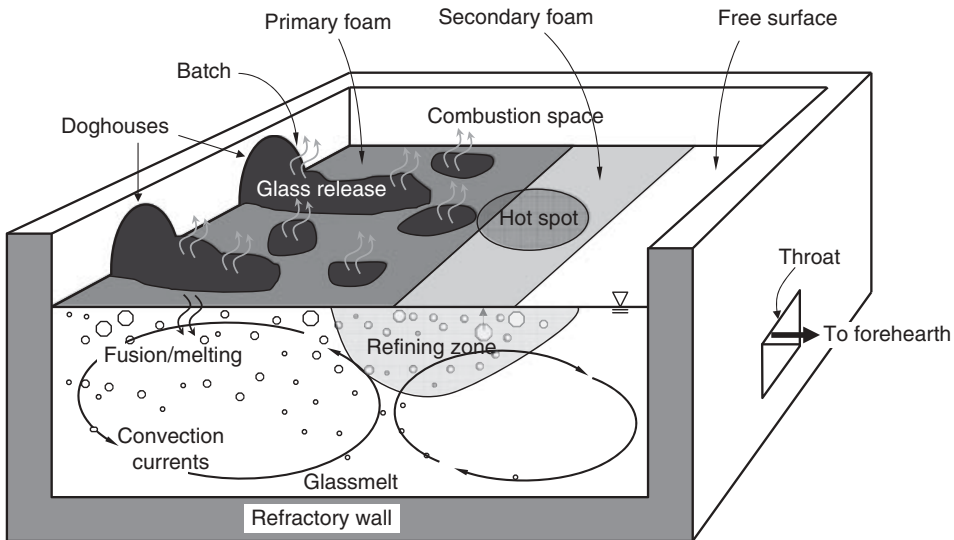


**Fig. 16.2** Schematic of a submerged throat glass melting tank showing primary and secondary foams [9, 25].



**Fig. 16.3** Photographs of the combustion space and the surface of the glassmelt in glass melting furnaces, transverse flames with batch logs, secondary foams, and free melt surface. Reproduced by permission of Research Association of the German Glass Industry (HVG) © 2010.

grade oxygen), (iii) flame direction (e.g., downward or sideways), and (iv) shape (e.g., cylindrical or flat). Heat transfer from the combustion space to the batch and to the glassmelt drives convection currents within the glassmelt to increase the retention time of the glass in order to achieve complete melting of raw materials, homogenization of the melt, and removal of gas bubbles from the melt prior to pulling it out for final processing.

The refractory walls thermally insulate the glassmelt. The furnace crown reradiates the thermal radiation from the flames to the floating batch and to the glassmelt surface. The batch can be introduced into the furnace either through inlet ports called doghouses from the back wall in the longitudinal direction (as shown in Fig. 16.2) or from the sides by using different types of chargers [4]. Due to density differences, the batch floats at the surface of the glassmelt where it spreads carried by the convection currents. The resulting batch coverage can assume many different shapes, from a uniform blanket to dispersed batch logs floating at the surface of the glassmelt. Figure 16.3 shows photographs taken in an actual industrial furnace featuring batch logs floating over the molten glass and so-called primary foam between the batch logs along with the so-called secondary foam and the glass free surface.

Glass melting tanks can be equipped with electric boosters or bubblers to enhance temperature uniformity and refining of the glassmelt. On the one hand, electric boosters provide additional energy for melting batch by passing an electrical current between electrodes inserted in the glassmelt and resulting in Joule heating [27]. On the other hand, bubblers inject large gas bubbles in the glassmelt in order to modify the convection

currents and further increase the residence time of the molten glass [28]. It also enhances heat transfer and glassmelt homogenization [23, 29]. Both electric boosting and air bubbling result in higher melt temperature, which accelerates the refining process as bubbles grow and rise more quickly to the glass surface [30]. Moreover, heat regeneration from the hot gases exiting the combustion space can be used as an energy saving measure to preheat the air or oxygen prior to combustion [4] and the batch before introducing it into the furnace [1].

Pilon *et al.* [31] showed that, for a specified heat input profile, the presence of glass foam in the submerged throat glass melting tank can significantly reduce the glassmelt temperature, which negatively affects the glass quality. More recently, Wang *et al.* [18] performed comprehensive three-dimensional numerical simulations of a 150 ton/day oxygen-fuel fired furnace consisting of coupled models for (i) the combustion chamber predicting the turbulent flow field along with temperature, combustion chemistry, and pollutant emission, (ii) the batch melting, (iii) velocity and temperature fields in the glassmelt, and (iv) foam treated as a static insulating layer with uniform thickness and known thermal conductivity. The authors established that the presence of foam over the glassmelt resulted in (i) increased temperatures of the crown, of the bottom furnace, and of the exhaust gas, (ii) lower glassmelt surface temperature, as well as (iii) larger net heat flux to the batch.

Finally, cold-top electric glass melters are commonly used for fiberglass and specialty glasses [2, 5, 21, 22]. Such melters are also used in nuclear waste vitrification [27, 32–36] where high level nuclear wastes are immobilized in borosilicate glasses [32, 33, 35]. Thermal energy required to melt the batch is entirely provided by electrodes submerged in the glassmelt [27, 37, 38]. This type of melter is typically smaller and more energy efficient than conventional fossil-fuel fired furnaces. They are also intrinsically cleaner since they do not emit  $\text{NO}_x$ ,  $\text{SO}_x$ , or dust [2]. Glass foam also forms in electric glass melters as a result of gas released and bubbles rising at the glassmelt surface. On the one hand, the glass foam reduces heat losses from the melt to the surroundings and thus increases the melt temperature [32, 34]. On the other hand, it acts as a thermal insulator between the hot glassmelt and the cold incoming batch loaded from the top [32, 34, 39, 40], thus reducing the batch melting rate [32, 34, 41]. In addition, higher melt temperatures result in more intense foaming due to the release of gases caused by (i) gas solubility typically decreasing with temperature [42], and (ii) thermally activated chemical reactions. Even in electric melters, the presence of foams has, overall, a detrimental impact on melter operation as excessive foaming slows down and may even halt the production process, resulting in losses in productivity and energy efficiency [32, 35].

## 16.1.2 Melting Chemistry and Refining

### 16.1.2.1 Redox State of Glass

The redox state of the glassmelt controls the refining reactions and the amount and gas species evolved [43–45]. The oxidation state of the glassmelt can be determined by considering the equilibrium between ferrous ( $\text{FeO}$ ) and ferric ( $\text{Fe}_2\text{O}_3$ ) oxides present in the glass, which may react according to

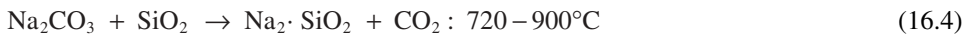


Thus, the oxidation state of the glass is directly related to the concentration or partial pressure of oxygen dissolved in the glassmelt [6], which can be measured using an oxygen sensor [46, 47]. The ratio of ferrous to ferric ions  $\text{Fe}^{2+}/\text{Fe}^{3+}$  in soda-lime-silica glass can be estimated from absorption measurements at 380 and 1060 nm wavelengths [48]. The redox state of the glassmelt can also be monitored by wet chemistry or Mössbauer spectroscopy [33]. Glass can be oxidized by adding oxidizing material to the batch, including sodium sulphate ( $\text{Na}_2\text{SO}_4$ ), cerium oxide ( $\text{CeO}_2$ ), iron oxides (e.g.,  $\text{Fe}_2\text{O}_3$ ), sodium and potassium nitrate ( $\text{NaNO}_3$  or  $\text{KNO}_3$ ), or oxidized glass cullets. Reducing conditions can be achieved by adding carbon, anthracite, chromite ( $\text{FeCr}_2\text{O}_4$ ), nitrates, and iron pyrite ( $\text{FeS}_2$ ) or reduced glass cullets [34, 43].

Green glasses owe their color to absorption by  $\text{Fe}^{3+}$  ions around 380 nm and to a lesser extent to absorption of  $\text{Fe}^{2+}$  at 1060 nm. Green glasses are typically oxidized glass, whereas blue glasses are mildly reduced due to an increasing amount of  $\text{Fe}^{2+}$  ions. Similarly, amber and dark amber glasses owe their color to the overwhelming presence of  $\text{Fe}^{2+}$  ions compared to  $\text{Fe}^{3+}$  and are referred to as reduced and strongly reduced glasses, respectively [43].

#### 16.1.2.2 *Melting Chemistry*

Melting of the batch is a complex physicochemical process that involves a large number of chemical reactions and phase transformations occurring over a wide range of temperatures [28]. The basic and most important reactions in the batch involve silica ( $\text{SiO}_2$ ), sodium carbonate ( $\text{Na}_2\text{CO}_3$ ), and calcium carbonate ( $\text{CaCO}_3$ ) as follows [43],



Large amounts of carbon dioxide ( $\text{CO}_2$ ) gas are produced as a result of the last three reactions. In fact, about 0.6 kg of  $\text{CO}_2$  are produced per kilogram of soda-lime silica glass [49] or 1440 liters of gas (at standard temperature and pressure) are produced per liter of soda-lime-silica glass [4]. The majority passes through the batch and escapes to the combustion space. Some of the produced  $\text{CO}_2$  diffuses into the melt [49]. A small fraction of the gas contributes to heterogeneous nucleation of bubbles within or just below the batch [50]. A fraction of these bubbles is entrapped in the batch and in the primary melt between the batch logs to produce the *primary foam* [43]. Bubbles generated at the bottom of the batch and too small to rise to the surface become trapped in the glassmelt and are carried with the convection currents.

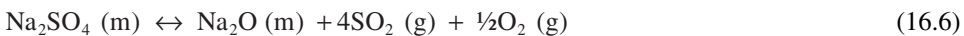
#### 16.1.2.3 *Refining Chemistry*

Refining agents are added to the batch to remove any bubbles from the glassmelt [49–52]. They mediate thermally activated redox reactions that produce or consume gases depending on the local conditions in the glass. In high temperature regions, the equilibrium of the refining reaction shifts to gas production [49]. Then, the refining gas produced diffuses from the molten glass into already existing gas bubbles. In addition, gases already contained in

bubbles are diluted by the incoming fining gas [30, 49]. This, in turn, enhances the diffusion of gases from the melt into the growing bubbles. Diffusion of fining gases makes bubbles grow in size until the buoyancy force is large enough to enable them to rise to the glassmelt free surface where they may aggregate and form foam. On the other hand, at low temperatures, the equilibrium of the fining reaction shifts to gas consumption, resulting in gas diffusion from the bubbles to the melt. Small bubbles, which did not yet grow to a sufficiently large size, then dissolve in the glassmelt [49, 53]. Note also that the solubility of refining gases in the glassmelt, most notably  $\text{SO}_2$ , decreases as temperature increases, thus enhancing gas transfer from the melt to the bubbles at high temperatures and from bubbles to glassmelt at low temperatures [19, 42].

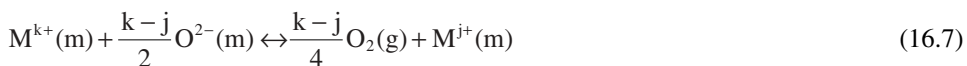
In practice, as the refining agents are carried by the glassmelt convection currents, they encounter high temperature regions (above  $1400^\circ\text{C}$ ) where refining reactions take place and refining gases are generated. These gases either form new bubbles through nucleation at the surface of unmelted batch particles [54] or dissolve in the glassmelt and eventually diffuse into existing gas bubbles. Such high temperature regions are typically encountered in the refining zone in the center of tank near the hot spot (see Fig. 16.2). Buoyancy enables sufficiently large bubbles to rise to the free surface of the glassmelt, where they accumulate and lead to the formation of *secondary foam* [43]. Refining reactions also take place in high temperature regions close to the tip of the batch.

Three types of refining agents are commonly used [43], namely (i) sulfates in the form of  $\text{Na}_2\text{SO}_4$ , (ii) variable-valence metal oxides, and (iii) halide compounds. Sodium sulfate ( $\text{Na}_2\text{SO}_4$ ) is the most commonly used refining agent and decomposes at high temperatures, around  $1400^\circ\text{C}$  in soda-lime-silica glass [4, 55], for example. It also accelerates the primary melt formation if introduced into the batch in suitable proportions [56]. Sodium sulfate is used in 90% of the glass produced worldwide for its relatively low cost [2, 4, 45]. Chemical reactions involving sulfates during glass melting have been the subject of intense studies [45, 49, 57]. In brief, sulfur is present in molten glass as sulfate ( $\text{SO}_4^{2-}$ ) or sulfite ( $\text{SO}_3$ ) under oxidizing conditions or as sulfide ( $\text{S}^{2-}$ ) under reducing conditions [55]. In oxidized melt at elevated temperatures, sodium sulfate undergoes the following reaction [55, 58],



where  $\text{SO}_2$  and  $\text{O}_2$  are released in the form of gases which dissolve in the glassmelt and diffuse into existing gas bubbles.

Variable-valence metal oxides refining agents include antimony oxide ( $\text{Sb}_2\text{O}_5/\text{Sb}_2\text{O}_3$ ), arsenic oxide ( $\text{As}_2\text{O}_5/\text{As}_2\text{O}_3$ ), and cerium oxide ( $\text{CeO}_3/\text{CeO}_2$ ) [51, 59]. As these refining agents encounter high temperature regions, they decompose according to the following equilibrium chemical reaction, written in a generalized form as [60]



In the case of antimony oxide, Kawachi and Kawase [50, 52] and Kawachi and Kato [61] showed that the rate of the forward reaction can be neglected in the production of TV panel glass. Therefore, the refining reaction is an irreversible decomposition of the refining agent generating  $\text{O}_2$  gas.

Finally, halide ions such as fluoride, chloride, bromide, and iodine ions evaporate at elevated temperatures rather than participate in refining reactions [62]. For example, sodium chloride is often used as a fining agent in borosilicate glasses by releasing HCl vapors [49].

#### 16.1.2.4 *Reduced-pressure Refining*

Another method for refining glasses consists of flowing the unrefined molten glass through a reduced pressure chamber using a siphon principle [63–68]. The low pressure causes bubbles to nucleate and grow rapidly to form foam. This process accelerates fining and can be implemented over small surface areas without requiring high temperatures [64], unlike the chemical refining previously discussed. In fact, it may not require additional heating of the melt, thus reducing the energy consumption. The refining process is favored by the melt expansion and foaming. However, the process throughput is limited by the amount of foam generated [69]. Indeed, glass foam can rapidly fill up the headspace of the vacuum chamber and hinder the process and limit the pressure reduction that can be achieved. Note that imposing near vacuum pressures over a large surface area and volume is very challenging and requires gas-tight container [69]. Thus, this method is limited to relatively small throughput furnaces.

### 16.1.3 Motivations

There are numerous fundamental and practical reasons for studying the formation and stability of glass foams appearing at different stages of the glass manufacturing process. They can be listed as follows [9]:

- **Energy efficiency.** According to indirect measurements and estimates by Trier [11], the resistance to radiative heating due to the presence of glass foam is significant. In fact, it could lead to a decrease by as much as 60% in radiative fluxes to the batch and glassmelt [11]. This results in significant reduction of the energy efficiency of the furnace and an increased fuel consumption [49, 70] in order to reach the glassmelt temperature required for refining and homogenization.
- **Glass quality.** Reduction in heat transfer from the combustion space to the glassmelt reduces the glass bath temperature and, hence, limits the rate of refining reactions, thereby increasing the number of bubbles and unmelted sand grains contained in the final product [70, 71].
- **Productivity.** The presence of primary and secondary foams at the surface of the glassmelt negatively impacts the productivity in many ways. It leads to an increase in the residence time of the glassmelt to reach the desired glass quality. In addition, primary foaming is also responsible for decreasing the batch melting rate [72]. Moreover, an increase in the pull rate favors foaming, thereby limiting the maximum pull rate allowed [43, 71]. Finally, extreme glass foaming can cause overflow of the melting tank and stop the production process altogether [32, 71].
- **Pollutant emissions.** Reflection and back-scattering of thermal radiation by glass foams result in a considerable increase in combustion-generated  $\text{NO}_x$  pollution, owing to an increase in the refractory's temperature by several hundreds of degrees Celsius [18, 49]. In addition, the presence of glass foam influences mass transfer of gas species (e.g.,  $\text{SO}_2$ ) from the molten glass to the combustion space. This affects furnace atmosphere composition and pollutant emission.

- Furnace integrity. The presence of foam enhances the refractory's attack at the metal-line [55] and also the wear of the crown due to increased temperatures [18, 70]. In addition, gas such as oxygen, water vapor, and sulfur oxide contained in foam bubbles tend to react with molybdenum and tungsten used as refractory metals for electrodes in all-electric or electric-boosted glass melting furnaces [73].
- New melting technologies. Led by economic and environmental concerns, new industrial practices use oxygen-fuel burners and significant amounts of recycled cullets in the batch. However, both of these measures have been shown to favor glass foaming [43, 55].

These issues underscore the critical importance of a detailed understanding of the formation and stability of primary and secondary glass foams not only for improving the process efficiency, reducing cost, and addressing environmental concerns associated with glass manufacturing but also for improving the quality of the final glass products. This chapter reviews the physical phenomena responsible for foam formation in glass melting furnaces. It also discusses experimental techniques used to investigate glass foams along with the resulting experimental observations. The associated physical models are presented and discussed in detail. Finally, strategies to mitigate the negative impacts of glass foams on operating cost, product quality, energy consumption, and pollutant emission are discussed.

## 16.2 Glass Foams in Glass Melting Furnaces

### 16.2.1 Primary Foam

Prior to melting, the batch goes through the heating and fusion stages, involving exo- and endothermic solid-state reactions between various batch components (eqn 16.2) [74]. As the temperature increases beyond 800°C, a liquid phase called primary melt begins to appear. As previously discussed, formation of the primary melt is accompanied by generation of significant amounts of carbon dioxide (eqns 16.3–16.5). A part of the released CO<sub>2</sub> is trapped in the viscous liquid phase, whereas the remaining gas percolates through the open channels present in the batch [34, 74]. As melting proceeds, the melt fraction and its connectivity increase, and the open pores get filled with molten glass whose viscosity is large at these relatively low temperatures [34]. Consequently, gas bubbles get trapped within the batch, resulting in batch expansion [74]. This phenomenon can be exacerbated when using cullets [43, 55]. Then, the batch may be covered by a layer of viscous melt preventing gases from escaping to the combustion space. In addition, the presence of trapped gases within the batch lowers its effective thermal conductivity and, in turn, reduces its melting rate [72]. Gas bubbles in primary foams contain CO<sub>2</sub> and CO and possibly other gases in lesser amounts depending on temperature, glass oxidation state, and batch composition and in particular its sulfate, nitrate, and carbon content [43, 44, 55].

### 16.2.2 Secondary Foam

Secondary foams are formed in glass melting furnaces due to gases generated by refining reactions responsible for bubble nucleation at the surface of unmelted grains that rise and

accumulate at the glass free surface [43, 55, 71]. In addition, bubbles trapped under the batch and carried by the convection currents eventually grow in the refining zone and rise to the glass free surface to contribute to secondary foaming [43]. It has been established experimentally that the secondary foam made of sulfate-refined glasses contains mostly  $\text{SO}_2$  and  $\text{O}_2$  in oxidized glass [49]. In reduced or mildly reduced glasses refined with sulfates,  $\text{S}_2$  is also present in the gas bubbles. In addition, secondary foams from glass refined with variable-valence metal oxides contain mainly  $\text{O}_2$ .

If the batch is heated at temperatures higher than  $1400^\circ\text{C}$  it undergoes two consecutive expansions: the first one is due to  $\text{CO}_2$  release, and the second is due to the generation of refining gases [55, 74]. Then, the “foaming temperature” refers to the temperature at which bubble generation becomes significant and foaming occurs [75]. A lower foaming temperature correlates with stronger glass foaming. Finally, note that in actual glass melting furnaces it is impossible to distinguish between primary and secondary foams as a continuous foam blanket covers part of the glassmelt.

### 16.2.3 Reboil

The term “reboil” is used to describe the reappearance of bubbles caused by supersaturation of gases physically or chemically dissolved within a previously refined and bubble free glass [8, 75]. In other words, bubbles form when the gas concentration dissolved in the molten glass exceeds its solubility at the local temperature and pressure. Reboil may occur upon heating after the glassmelt has been refined and cooled down. It can also be induced by lowering the pressure above the melt or by stirring the glassmelt [76]. Reboil is caused by gases whose solubility in the melt (i) decreases with temperature and/or pressure [8] and (ii) is relatively large so that large volume of gases can be released during reheating and/or pressure reduction [77]. This is the case of water and  $\text{SO}_3$ , which rapidly decomposes in  $\text{SO}_2$  when released from the melt into gas bubbles [45]. Reboil can also occur when oxidized and reduced glasses are brought into contact due to the mismatch in their gas solubility [8].

In glass melting furnaces, reboil may occur in the forehearth due to reheating or stirring [76]. Indeed, after the glassmelt has been refined at relatively high temperature, it cools down as it flows out of the furnace through the throat. It is then reheated in the forehearth before being formed.

Quantitatively, reboil is assessed through the so-called “reboil temperature” corresponding to the temperature above which bubbles start forming typically under atmospheric pressure. Similarly, the so-called “reboil pressure” is the reduced gas pressure below which bubbles appear under isothermal conditions [32, 76]. In reboil, bubbles form due to heterogeneous nucleation often taking place at the melt/refractory interface [77, 78]. Reboil and foaming differ in the intensity of the gas release rate, in the volume fraction occupied by gas bubbles, and in the bubble size and the distance separating them [77]. Thus, reboil and glass foaming should not be confused and reboil is not discussed further in this chapter.

In summary, Table 16.1 presents the different type of glass foams encountered in glass melting furnaces, the source of gases, the bubble size, and the furnace location where each type may be found.

**Table 16.1** Summary of the different types of glass foams encountered in glass melting furnaces.

Foam type	Gas source	Gas species	Bubble size	Location
Primary	Batch melting and refining reactions	CO <sub>2</sub> , N <sub>2</sub> , CO, SO <sub>2</sub>	Small	Around batch logs
Secondary	Refining reactions	CO <sub>2</sub> , SO <sub>2</sub> , O <sub>2</sub> , S <sub>2</sub> , HCl	Large	Refining zone

### 16.2.4 Parameters Affecting Glass Foaming

The formation and stability of glass foams are affected by obvious parameters such as temperature and glassmelt composition which determine its properties, including viscosity, surface tension, and gas solubility. They also depend on bubble size distribution, bubble generation rate or gas flow rate to the glassmelt surface. If it were only for these parameters, glass foams would behave similarly to any other foams, including aqueous foams, which have been investigated extensively. Understanding glass foams is complicated by the facts that they are also affected by complex and intimately coupled phenomena such as (i) the oxidation state of the glass as its components are involved in numerous reversible redox reactions, (ii) the amount of dissolved gases in the glassmelt, (iii) the refining agent and the associated thermally activated reactions, (iv) the batch composition (cullets, sulfates) and its conditioning (grain size, heat treatment, or compaction), (v) the composition and pressure of the atmosphere above the foams, and (vi) the temperature history of the batch.

These elements are related in complex ways to operating parameters of the glass melting tank such as (i) the use of recycled and contaminated cullet of mixed colors, (ii) the type and amount of refining agents added to the batch, (iii) the furnace pull rate, (iv) the combustion fuel and oxidizer and the atmosphere composition, (v) the heat flux incident on the foam from the combustion space and the crown, (vi) the potential temperature gradient across the foam, and even (vii) the luminosity of the flame [79, 80].

Figure 16.4 summarizes the different parameters affecting glass foams forming in glass melting furnaces. It aims to illustrate the diversity and complexity of the physical phenomena responsible for glass foaming. This may also explain why predicting the behavior of glass foams and controlling foaming in industrial furnaces has remained elusive, as discussed in the following sections.

## 16.3 Physical Phenomena

### 16.3.1 Glass Foam Physics

#### 16.3.1.1 Mechanisms of Foam Formation

A number of intimately interacting physical phenomena govern the dynamics of glass foam formation and decay as well as its steady-state behavior. They include (i) bubble built-up in the foam due to the bubble influx from the bottom of the foam layer, (ii) drainage of the

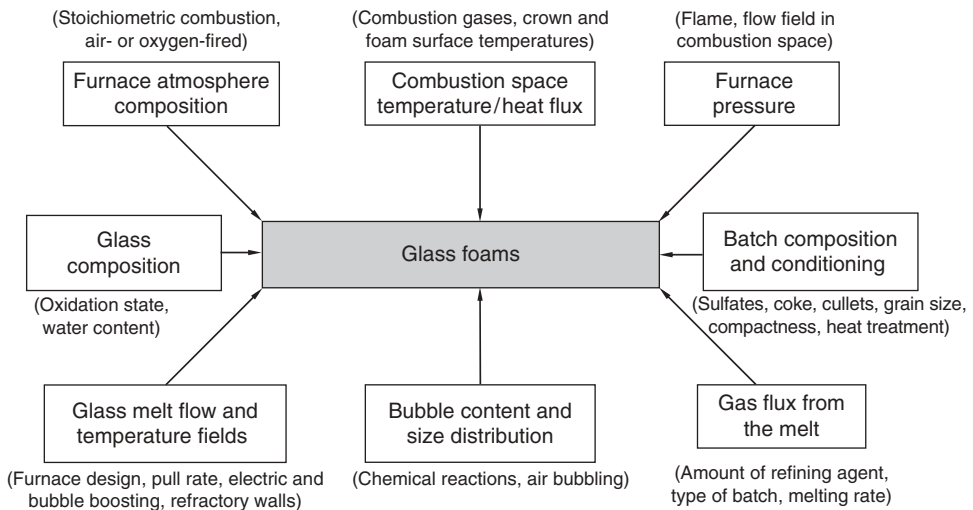


**Fig. 16.4** Schematic of the various parameters affecting primary and secondary glass foams.

molten glass from the Plateau borders, (iii) gravity-induced drainage of the liquid from the foam through the Plateau border channels, (iv) abrupt liquid discharge within the foam due to the rupture of the lamellae and coalescence of adjacent bubbles, and (v) so-called bubble disproportionation or Ostwald ripening caused by interbubble gas diffusion from smaller bubbles (higher pressure) to larger bubbles (lower pressure) [39, 81, 82]. Different mechanisms dominate the life of a bubble as it moves from the bottom to the top of the foam. Initially, foam growth is primarily defined by the balance between the bubble build-up and the liquid drainage from Plateau borders and Plateau border channels. However, near the top of the foam where liquid lamellae separating the bubbles are sufficiently drained, bubble coalescence and interbubble gas diffusion tend to dominate. The above phenomena also take place in aqueous foams. However, glass foams differ from aqueous foams in the following ways:

1. The formation and stability of aqueous foams is associated with the formation of an electrical double layer at the gas–liquid interface due to the presence of surfactant molecules. However, it is unclear whether such a phenomenon takes place in glass foams [78].
2. On the other hand, the viscosity of the glassmelt is large and depends strongly on temperature and glassmelt water content [71, 83–85].
3. Volatilization of some components of the glassmelt due to large temperatures is a critical phenomenon [49, 71].
4. Glass foams are very good thermal insulators and are, in practice, subject to very large temperature gradients.
5. Glass foaming also strongly depends on the redox state of the melt and on chemical reactions taking place between the different components of the melts and the gases released by chemical reactions and/or present in the atmosphere above the foam.
6. The formation of primary foams is affected by the presence of unmelted sand grains, which may stabilize or destabilize the bubble interface [35, 86].

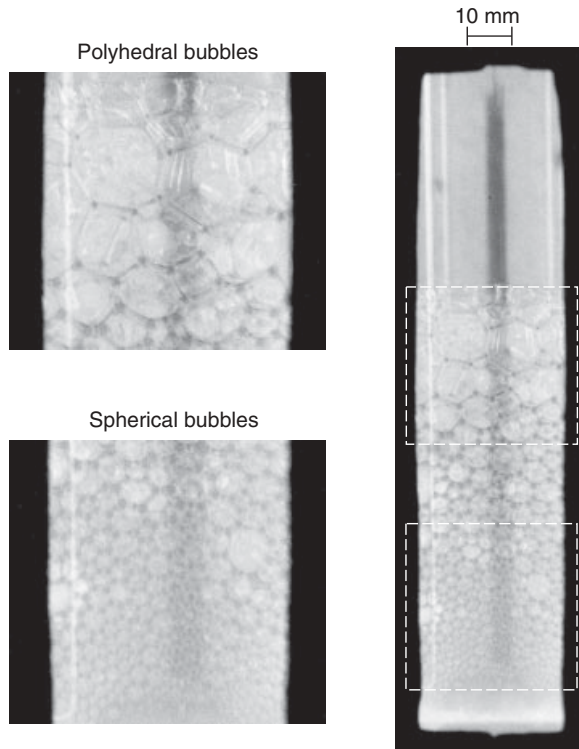


**Fig. 16.5** Photographs of spherical and polyhedral bubbles in glass foams generated from soda-lime-silica glass by sulfate thermal decomposition at 1480°C. Reproduced by permission of Paul Laimböck © 1998.

### 16.3.1.2 Glass Foam Morphology

Glass foams consist of an ensemble of bubbles whose size distribution function varies across the foam layer. The bubbles at the bottom of the foam layer are usually spherical in shape, and their size distribution is primarily determined by how they were generated and the history of their transport through the melt. The bubbles at the top of the foam layer are usually polyhedral, and their geometry typically obeys Plateau's laws [82]: (i) three and only three films or lamellae, called Plateau borders, meet at an edge of a polyhedral bubble at an angle of 120°, and (ii) four and only four edges, called Plateau border channels, meet at a point at an angle of 109°. The dodecahedron nearly satisfies Plateau's laws and, thus, is commonly used as an idealized model for polyhedral bubbles in the foam. Laimböck [43] observed both spherical and polyhedral bubbles in glass foam generated by sulfate thermal decomposition in soda-lime-silica glass in laboratory experiments as illustrated in Fig. 16.5. Similar observations were made in foams scooped from industrial glass furnaces [44] and laboratory experiments [71]. Bubbles generated by chemical reactions are typically much smaller than those generated by gas injection in the laboratory system. Glass foams

generated in the laboratory by bubbling gas through the melt at 1400°C have a typical diameter between 15 and 20 mm [43]. Finally, the thickness of the lamellae separating two adjacent bubbles in glass foams was observed to be about 100 nm [43, 71, 79].

### 16.3.2 Surface Active Agents and Surface Tension of Gas/Melt Interface

Surface active agents are elements whose addition to the glassmelt in small amounts reduces surface tension. They, in turn, increase the stability of the bubbles and tend to inhibit bubble coalescence. Elements in the composition of the glass have been identified as surface active agents. For example, Cooper and Kitchener [79] suggested that  $P_2O_5$  and  $SiO_2$  in the  $CaO-SiO_2-P_2O_5$  system could be treated as surface active agents since they were found to adsorb at the melt surface and lower its surface tension for various  $CaO/SiO_2$  ratios. In fact, these glasses were shown not to foam significantly unless they contained more than 67 wt%  $SiO_2$  and 1–2 wt%  $P_2O_5$ . Cooper and Kitchener [79] also mentioned that  $B_2O_3$  and less significantly  $Al_2O_3$  acted as surface active agents while  $TiO_2$  did not. In addition, Kucuk *et al.* [87] showed that  $MoO_3$ ,  $Rb_2O$ ,  $B_2O_3$ ,  $K_2O$ , and  $PbO$  reduce the surface tension of silicate melts. Finally, silanol groups  $Si-OH$  formed by reaction with water vapor contained in the bubbles have also been identified as surface active agents in molten glass [88].

Laimböck [43] also measured the composition across a quenched vertical film of soda-lime-silica glass. He showed that the film surface was enriched in  $Na_2O$  and became depleted in  $CaO$  and  $SiO_2$ . The surface tension decreases with increasing  $Na_2O$  and decreasing  $CaO$  and  $SiO_2$ . Thus,  $Na_2O$  behaves as a surface active agent. These results confirmed earlier measurements by Kappel and Roggendorf [89].

Moreover, Bindal *et al.* [35] investigated three-phase foaming by heating a mixture of precipitate hydrolysis aqueous (PHA) and sludge-simulating plutonium/uranium extraction (PUREX) nuclear waste. Upon heating, the sludge boiled at around 102°C and gases were generated, resulting in foaming. The authors established that foams made of liquid containing fine solid particles can be stabilized by the particles based on the following two mechanisms:

1. **Adsorption of biphilic particles** at the gas–liquid interface. As the liquid drains, the particle concentration increases and steric repulsion between particles on each face of the liquid film stabilizes the bubble lamellae and in turn the glass foams [35].
2. **Layering of solid particles** inside the liquid film separating the gas bubbles caused by the confinement of the particles in the films. This results in long-range forces that stabilize the bubble lamellae [35].

Finally, the composition of the gas phase in contact with the melt also affects the surface tension of the glassmelt/gas system. According to Parikh [90], polar gases such as sulfur dioxide ( $SO_2$ ), ammonia ( $NH_3$ ), hydrogen chloride ( $HCl$ ), and water vapor ( $H_2O$ ) lower the surface tension of soda-lime-silica glass, whereas non-polar gases such as dry air, dry nitrogen, helium, and hydrogen have no effect. Among the polar gases cited, water has the largest dipole moment and therefore has the strongest effect on surface tension [90]. In fact, Parikh [90] showed that the surface tension of soda-lime-silica glass decreases with the square root of the partial pressure of water vapor.

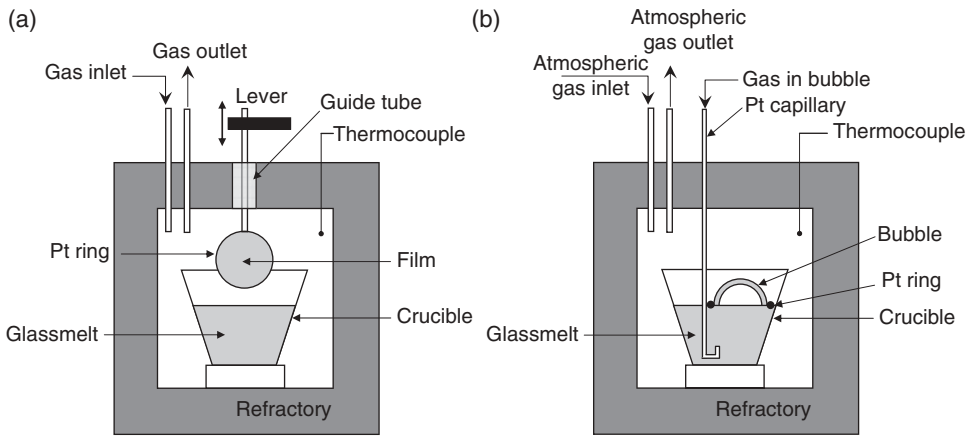


**Fig. 16.6** Schematic of the experimental apparatus used to study (a) liquid drainage and stability of a vertical molten glass film and (b) the lifetime of a single bubble formed from molten glass [43, 71].

### 16.3.3 Drainage and Stability of a Single Molten Glass Film

Figure 16.6a shows a schematic of a typical experimental apparatus designed to investigate the drainage and stability of a vertical single liquid film [43, 71]. Kappel *et al.* [71] used such an apparatus to investigate a single vertical molten glass film made of soda-lime-silica glass between 990 and 1100°C and under various atmosphere compositions. The single film was created by dipping a Pt ring into molten glass. First, the authors established that the film thickness  $\delta(t)$  decreased exponentially with time according to  $\delta(t) = \delta(0)\exp(-k_L t)$  where  $k_L$  varied with temperature, glass and atmosphere compositions. As expected, the film drainage was faster as the temperature increased. However, this could not be solely attributed to the exponential decrease of melt viscosity with temperature. More importantly, the film drainage halted for thickness around 100 nm and could be stable for nearly one hour. Lamellae of similar thickness were also observed in glass foams made of soda-lime-silica glass [71] and silicate glass [79]. In addition, the presence of water vapor in the atmosphere did not affect the film drainage. This is in contradiction with what was observed for foam made of the same glass [71].

Moreover, Kappel *et al.* [71] investigated film stability by blowing hot nitrogen gas, under different pressure or flow rates, directly at the film for different furnace temperatures. The authors showed that the average lifetime of a drained film decreased exponentially with gas pressure and almost linearly with temperature [71]. The authors concluded that tearing of the film was independent of the drainage even though the film had to be thin enough to break. Thus, the lifetime of a molten glass film depends on two independent time scales: the drainage time and the lifetime of the critically thin film [39].

Finally, Laimböck [43] performed similar experiments to those reported by Kappel *et al.* [71] for vertical lamellae drawn from (i) oxidized soda-lime-silica melts without and with sulfate in the form of  $\text{SO}_3$  and (ii) reduced soda-lime-silica melts with sulfate in the form of  $\text{S}^{2-}$ . He also observed that the lifetime of the lamellae from all melts decreased as

the temperature increased. In addition, the lifetime of the film was found to decrease significantly as dissolved  $\text{SO}_3$  content in oxidized soda-lime glass increased. In fact, a sulfate gall was observed at the film surface below 1300–1350°C, which either destabilized the film or prevented its stabilization. In general, gall formation occurred in oxidized glass below 1300°C and varied with sulfate concentration, temperature, and glass oxidation state. Gall formation was observed neither in sulfate-free oxidized glass nor in reduced glass. Above 1300°C, the gall disappeared due to the dissolution and volatilization of sulfate, which created fluid flow in the glassmelt similar to Marangoni flows [43].

### 16.3.4 Gas Bubbles in Molten Glass

#### 16.3.4.1 Bubble Nucleation

Heterogeneous bubble nucleation can occur on the surface of undissolved sand grains or on refractory walls due to local supersaturation of the glassmelt with gases [49]. Němec [54] experimentally observed, under uniform temperature conditions, that heterogeneous bubble nucleation occurs at the surface of undissolved sand grains only if a refining agent is present, while homogeneous bubble nucleation could never be observed. It indicates that bubble nucleation takes place if the glassmelt is supersaturated with refining gases. Cable and Rasul [78] reported that heterogeneous bubble nucleation occurred at the surface of the refractory even at small supersaturation. Finally, Roi *et al.* [91] discussed bubble generation and the formation of a bubble curtain consisting of very small bubbles close to the refractory walls.

#### 16.3.4.2 Stability of a Single Bubble at the Glassmelt Surface

Figure 16.6b shows a schematic of an experimental setup for studying the stability of a single bubble at rest at the surface of molten glass as described by Kappel *et al.* [71]. The single bubble can be formed by injecting an arbitrary gas inside the molten glass through a Pt capillary. A Pt ring, placed on the glassmelt free surface, prevents the bubble from drifting. Finally, the composition of the furnace atmosphere can be controlled by injecting any arbitrary gases and can be different from the gases contained inside the bubble.

Kappel *et al.* [71] investigated single bubbles formed at the surface of molten soda-lime-silica without and with addition of  $\text{Na}_2\text{SO}_4$  and of reduced brown glass. The furnace temperature was 1100°C and its atmosphere consisted of humid air while the bubbles contained air,  $\text{N}_2$ ,  $\text{CO}_2$ , or  $\text{SO}_2$ . For reduced brown glass and soda-lime-silica with or without sulfates, air bubbles were found to be more stable than those filled with  $\text{N}_2$  and  $\text{CO}_2$ . In all cases,  $\text{SO}_2$ -containing bubbles were the most unstable regardless of the sulfur content and redox state of the glass. In addition, the lifetime of a single air bubble on soda-lime-silica glass decreased from about 300 to 30 seconds when the glass was refined with sulfate. Laimböck [43] attributed these observations to the formation of a destabilizing sulfate gall at the surface of bubbles below 1300°C as previously discussed for vertical films. In addition, the authors established that replacing the air furnace atmosphere by  $\text{N}_2$  and  $\text{CO}_2$  had no effect on the bubble stability [71].

Note that Debrégeas *et al.* [92] performed similar experiments with single air bubbles made from pure and uncontaminated polydimethylsiloxane (PDMS) at room temperature.

The authors observed that the metastable film thickness at the top of the bubble was about 70 nm when the bubble burst. The characteristic drainage time was found to be  $\tau = \mu/\rho gr$  where  $\mu$  and  $\rho$  are the dynamic viscosity and density of the fluid while  $g$  and  $r$  are the gravitational acceleration and the cap bubble radius, respectively. The authors demonstrated that a single bubble can be stable for several minutes thanks to PDMS's high viscosity ( $\approx 103$  Pa.s) and despite the absence of surface active agents.

Finally, some experimental observations made on single molten glass films or bubbles contradict well known observations made with glass foams in the laboratory and in industrial furnaces. This led Cooper and Kitchener [79] and Kappel *et al.* [71] to question the approach of extending experimental observations on a single film or bubble to predicting the behavior of glass foams.

#### 16.3.4.3 Bubble Rise through Molten Glass

Studies of the bubble motion have been concerned mainly with a single bubble rising in an infinitely large quiescent pool of molten glass under uniform temperature. In brief, if the bubble is small and/or its surface is contaminated, no gas circulation takes place inside [93]. Then, the bubble behaves like a solid sphere (immobile interface) and rises in the molten glass with the relative vertical terminal velocity given by Stokes's law [93],

$$w_r = \frac{2}{9} \frac{\rho g r}{\mu}, \quad (16.8)$$

where  $\rho$  and  $\mu$  denote the density and viscosity of the glassmelt while  $r$  is the bubble radius and  $g$  is the gravitational acceleration.

On the other hand, if the spherical bubble is large and/or its surface is contamination-free, the vertical terminal velocity, relative to the molten glass, follows the Hadamar-Rybczynski formula [93–95],

$$w_r = \frac{1}{3} \frac{\rho_\infty g r^2}{\mu_\infty}. \quad (16.9)$$

Experimental results suggested that the velocity of bubbles with diameter larger than 1 mm satisfies eqn (16.9) while smaller bubbles rise with velocity given by eqn (16.8) [95]. Similarly, Jucha *et al.* [93] established that the Hadamar-Rybczynski formula was valid for bubbles larger than 10  $\mu\text{m}$  rising in borate glass at temperatures between 800 and 1000°C.

The bubble rise in the glassmelt is complicated by gas diffusion in and out of the bubble, which changes its size and therefore the buoyancy force. Numerous studies have investigated the shrinkage or growth of a stationary bubble containing a single gas [96, 97], sometimes accounting for refining reactions [59, 98]. Other studies were concerned with the growth of a stationary bubble containing several gases with or without refining reactions [98–100]. More realistic situations were investigated by accounting for the bubble rise due to buoyancy for a single gas bubble [101, 102] or a bubble containing several gases [103, 104], including the presence of refining reactions [51, 62, 105].

Even though modeling the behavior of individual bubbles provides insight into the mechanism of bubble generation, motion, growth, and shrinkage, it does not predict the

**Table 16.2** Summary of experimental studies of glass foams reported in the literature.

Glass	Batch or gas in bubble	Gas source/method	Heating	Temperature (°C)	Atmosphere	Ref.
Soda-lime, brown, E-glass, crystal, borosilicate (decay)	Culletts compressed at 2.5 MPa	CaCO <sub>3</sub> or Na <sub>2</sub> CO <sub>3</sub>	Isothermal	1000–1200	Dry/wet air N <sub>2</sub> + SO <sub>2</sub> Air + NH <sub>3</sub>	[71]
Sodium, lithium, potassium silica	Melted glass	Na <sub>2</sub> SO <sub>4</sub>	Heat ramp (3–4°C/min)	1100–1500	N <sub>2</sub> , N <sub>2</sub> -H <sub>2</sub> , CO <sub>2</sub> SO <sub>2</sub> , dry/wet O <sub>2</sub>	[77]
Sodium, lithium, potassium silica	Premelted glass cullet	Na <sub>2</sub> SO <sub>4</sub>	Heat ramp (3–4°C/min)	1150	N <sub>2</sub> , N <sub>2</sub> -H <sub>2</sub> , CO <sub>2</sub>	[78]
Soda-lime silica	Loose	Na <sub>2</sub> SO <sub>4</sub>	Heat ramp (3–4°C/min)	Up to 1515	N <sub>2</sub> , N <sub>2</sub> -H <sub>2</sub> , CO <sub>2</sub> dry/wet O <sub>2</sub>	[75]
Sheet glass Fiberglass	Loose Loose with fine or coarse grains	0–13 wt% Na <sub>2</sub> SO <sub>4</sub> Fluorine	Isothermal Time gradient method	1450, 1480 1500	Air Air	[20] [70]
Simulated nuclear waste with borosilicate	Loose/compacted Cold/pre-heating	Variable-valence metal oxides	Heat ramp (5–10°C/min)	500–1150	Air	[72]
Soda-lime silica (with Al <sub>2</sub> O <sub>3</sub> , SrCO <sub>3</sub> )	Loose	Na <sub>2</sub> SO <sub>4</sub>	Isothermal or heat ramp (14°C/min)	1400 or up to 1450	Air	[74]
Soda-lime silica (with Al <sub>2</sub> O <sub>3</sub> )	Loose (coarse or fine)	Na <sub>2</sub> SO <sub>4</sub>	Isothermal	1400–1480	Air	[113]
Soda-lime silica (with Al <sub>2</sub> O <sub>3</sub> )	Loose (coarse or fine)	Na <sub>2</sub> SO <sub>4</sub>	Heat ramp (14°C/min)	Up to 1450	Air	[114]
Soda-lime silica (oxidized or reduced)	Loose (with or without culletts)	Na <sub>2</sub> SO <sub>4</sub>	Heat ramp	Up to 1500	Dry/wet air	[43]
E-glass	Loose	Na <sub>2</sub> SO <sub>4</sub>	Heat ramp (5–10°C/min)	Up to 1500	CO <sub>2</sub> , O <sub>2</sub> , air, H <sub>2</sub> O mixtures	[115]
Soda-lime silica	Loose	Na <sub>2</sub> SO <sub>4</sub> with carbon	Heat ramp (10°C/min)	1300, 1400, 1500	Wet air (11–100 vol.%)	[57, 116]
E-glass	Loose	Na <sub>2</sub> SO <sub>4</sub>	Heat ramp (10°C/min)	Up to 1250 and 1500	2% O <sub>2</sub> + 55% H <sub>2</sub> O	[46]
Soda-lime silica (various SO <sub>3</sub> wt%)	Molten glass	Gas injection (air)	Isothermal	1425–1500	Air	[43]
Float glass	Molten glass	Gas injection (N <sub>2</sub> , CO <sub>2</sub> )	Isothermal	1300 or 1400	Air	[117]
Silicate slag (decay)	Molten slag (CaO-SiO <sub>2</sub> + P <sub>2</sub> O <sub>5</sub> )	Gas injection (10% H <sub>2</sub> -90% N <sub>2</sub> )	Isothermal	1500–1750	10% H <sub>2</sub> -90% N <sub>2</sub>	[79]
Flat, optical, wool glass (decay)	Melted glass	Reduced pressure method	Isothermal	1200–1500	Air (50–750 mmHg)	[70]
Iron alkali borosilicate	Culletts	Reduced pressure method	Isothermal	1150	Air (0–1 bar)	[32]

volumetric gas flow rate and size distribution of bubbles rising to the surface of the glassmelt to form glass foams. However, it can be used to trace individual bubbles introduced at the batch/glassmelt interface and predict their growth and shrinkage as they are transported through regions with different temperatures, gas concentrations, and pressures [30, 49, 50, 52]. Alternatively, Ungan *et al.* [106] solved the conservation equation for the total number of bubbles and took into account the effect of bubbles on the flow and temperature fields of the molten glass through the reduction of the effective density of the two-phase mixture. By contrast, population balance theory [107] enables one to predict in detail the radius and gas content of polydispersed bubbles and their density function throughout the glass melting tank. A limited number of studies have applied population balance theory to the bubble dynamics in glass melting tanks in 2D or 3D with various assumptions and different levels of refinement [108–112]. The latter studies enable the prediction of the local superficial gas velocity reaching the glassmelt surface, which can then be used in dynamic or steady-state models described in Section 16.5.

## 16.4 Experimental Studies

### 16.4.1 Introduction

As previously discussed, it is of fundamental and practical interest to understand each type of glass foaming process and to predict (i) the conditions under which glass foam forms, (ii) how fast it grows and decays, and (iii) how stable it is under various conditions in order to operate the process in an optimum manner.

Table 16.2 summarizes laboratory experiments performed to investigate the effect of the numerous parameters affecting glass foam formation and stability summarized in Fig. 16.4. Most of the studies focused on soda-lime-silica glass, E-glass, and borosilicate glasses as well as binary glasses. The majority of the studies investigated glass foams created by ramp-heating of a batch under different heating rates. Both fine and coarse batch grains were investigated. In addition, steady-state and transient decay of glass foams were typically studied under isothermal conditions. Most experiments were performed under atmospheric pressure and various atmosphere compositions.

Figure 16.7 shows a typical experimental setup used to study both primary and secondary glass foams [115, 118]. Typically, glass foaming is performed in a furnace with a fused quartz window on the front door enabling visual access inside the furnace. The sample height is recorded over time with a visual or infrared video camera and filters. The furnace can be equipped with a rear recess kept at a temperature lower than that of the crucible to provide a darker background for a better contrast [115]. The furnace atmosphere can be controlled by injecting different gases or gas mixtures at predetermined temperatures. In particular, furnace humidity can be controlled by bubbling compressed gas through water in a flask kept at a constant temperature [43, 71, 75, 77, 78, 115], as illustrated in Fig. 16.7. The temperature of the incoming atmospheric gas can also be controlled by heating the gas line with an insulated resistive heating coil wrapped around the gas tube. This also helps prevent water condensation in the gas inlet system when wet atmospheres are tested [115].

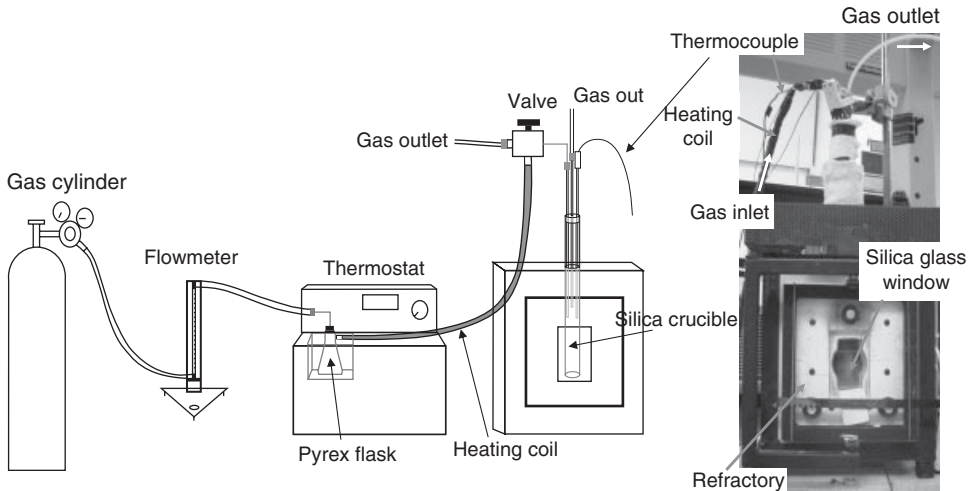


**Fig. 16.7** Schematic of typical experimental apparatus used to investigate glass foaming along with photographs of the furnace used by Kim et al. [115, 118].

## 16.4.2 Transient Primary and Secondary Glass Foams

### 16.4.2.1 Experimental Apparatus and Procedure

Figure 16.8a shows the inside of the furnace used to study the dynamic behavior of glass foaming. In this method, the batch is placed as a loose or compacted blanket in a transparent crucible (e.g.,  $\text{SiO}_2$ ) tall enough to contain the glass foam. Foaming is achieved by increasing the batch temperature either by ramp-heating the furnace or by placing the crucible inside a pre-heated isothermal furnace. Glass foams are produced as a result of gas generation due to batch conversion and refining. This method results in glass foam that grows and eventually collapses when all the gas generating reactions end [71, 74, 75, 77, 78, 113–115]. In other words, the glass foam height continuously changes over time and never reaches a steady state. This method can simulate growth and decay of primary and secondary foams depending on the maximum temperature reached [43, 115].

Alternatively, Cable and co-workers [75, 77, 78] used an apparatus similar to that depicted in Fig. 16.8a to investigate secondary foaming with the capability to vary the atmosphere composition and control the heating rate. First, the authors melted glass in air in a separate electric furnace at different temperatures (1200–1400°C) and for various durations (5–28 h) until the glass melt was free of bubbles. The produced melts were cooled and stored in desiccators. The produced glass was then crushed into 5–10 mm pieces and then used for secondary glass foaming experiments to measure the foaming temperature for various conditions.

Moreover, Gerrard and Smith [70] described a reduced pressure apparatus where the batch was introduced into a crucible placed in a furnace with prescribed temperature and pressure. The pressure of the atmosphere above the sample was controlled by evacuating the furnace with a vacuum pump. Visual access was possible through a quartz window to

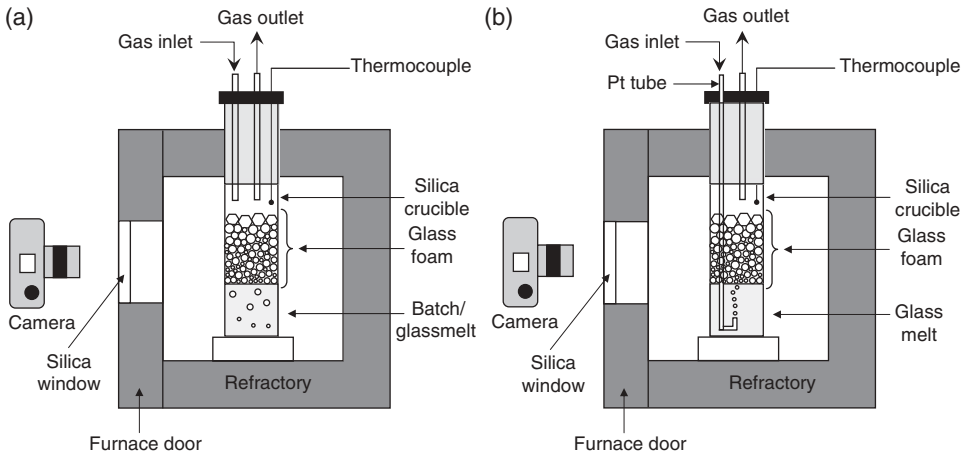


**Fig. 16.8** Schematic of experimental setup used to study (a) batch melting with primary and secondary foaming and (b) foaming by gas injection. Visual access and video recording are made possible through a glass window on the furnace door.

monitor foaming. The batch was first melted between 1200 and 1500°C at atmospheric pressure. After an arbitrary melting time, the pressure was reduced until foaming was observed corresponding to the reboil pressure. The authors also used this apparatus to monitor the decay of the glass foam. Similar experimental setup and procedure were used by Goldman *et al.* [32].

Finally, Gerrard and Smith [70] proposed an alternative setup to investigate primary foaming. Their experimental procedure consisted of continuously introducing, with an arbitrary speed, loose batch placed in a rhodium or platinum “boat” into a pre-heated furnace at constant temperature in an atmosphere with arbitrary composition. After a few minutes, the boat was withdrawn from the furnace and cooled. This procedure was meant to reproduce the temperature history of the batch from the time it is introduced in the furnace until it melts. It is commonly used in industry to assess the effect of different batch compositions and process parameters. Unfortunately, this method can only provide qualitative results, as acknowledged by Gerrard and Smith [70].

#### 16.4.2.2 Experimental Observations

Figure 16.9 shows typical experimental results of transient foaming experiments (Fig. 16.8a). It plots the batch/foam height and furnace temperature as a function of time for 4 g of loose batch of E-glass batch containing sulfate ramp-heated at 5°C/min up to 1500°C [115]. As the temperature increased, the volume of the sample decreased slightly as sintering and gas release took place. Around 1100°C the batch started melting, resulting in a dramatic reduction in sample thickness. Shortly thereafter, the melt thickness increases as CO<sub>2</sub> bubbles are generated and get trapped in the molten glass and expand due to CO<sub>2</sub> generated by fusion reactions (period I). This is followed by a rapid growth around 1400°C (period II) caused by the release of fining gases, SO<sub>2</sub> in this case. Similar plots have been reported throughout the literature for different glass compositions and heating rates [43, 49, 72, 74, 117].

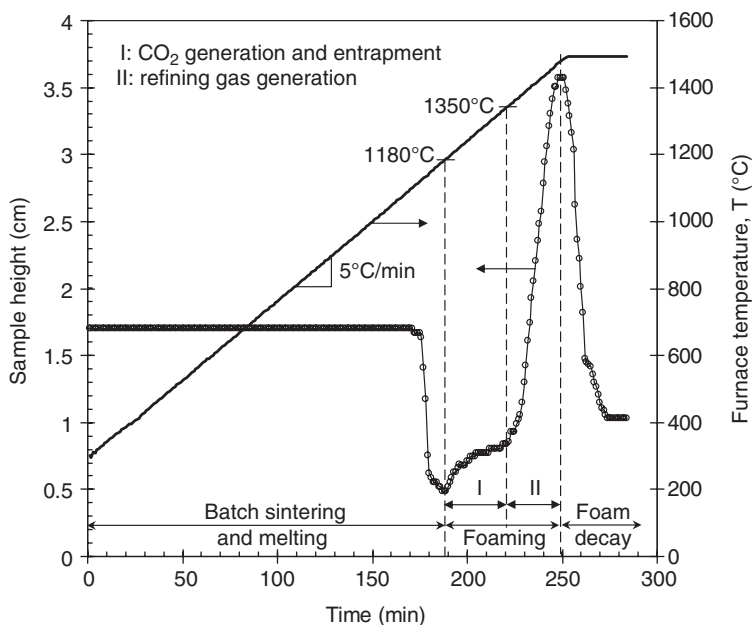


**Fig. 16.9** Temporal evolution of sample height and furnace temperature during primary foaming of E-glass batch ramp-heated at 5°C/min [115].

The following subsections review studies investigating the effects, on glass foaming, of (i) temperature and heating rate, (ii) redox state, (iii) batch preparation, (iv) batch and glass compositions, (v) sulfate addition, as well as (vi) atmosphere composition and pressure.

**Effect of Temperature and Heating Rate.** Laimböck [43] performed a thorough study of the effect of redox state on glass foaming. The author melted oxidized soda-lime-silica batch containing 1.0 wt% of  $\text{Na}_2\text{SO}_4$  at a constant heating rate of 4°C/min up to 1465, 1480, and 1500°C. He observed that secondary foaming and sulfate losses were larger as the final temperature increased. This can be explained by the fact that beyond the refining temperature (~1400°C in this case), more and more refining gases ( $\text{SO}_2$  and  $\text{O}_2$ ) are generated by thermal decomposition of refining agents ( $\text{Na}_2\text{SO}_4$ ). In addition, under a constant heating rate, it takes longer to reach a higher final temperature, thus giving more time for the refining reactions to proceed.

Moreover, Fig. 16.10a shows the ratio of volume of gas in the foam  $V_{\text{gas}}$  to the volume of soda-lime-silica melt  $V_{\text{melt}}$  denoted by  $\Psi = V_{\text{gas}} / V_{\text{melt}}$  as a function of temperature between 1250 and 1500°C for three different heating rates namely 5, 10, and 15°C/min as reported by Kim *et al.* [58, 115]. It establishes that glass foaming increases as the heating rate increases [115].

Mrna [58] distinguished between (a) surface foams observed at low heating rates and (b) bulk foams observed under high heating rates and in a deep enough container. Surface foams consist of three stratified layers: (i) a bubble-free melt, (ii) a bubbly layer, and (iii) the glass foam layer. On the contrary, bulk foams consist of bubbles expanding

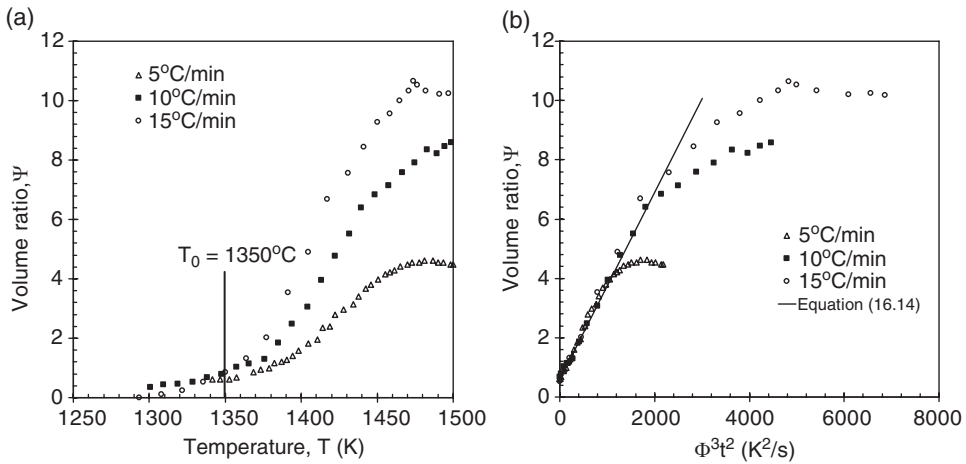


**Fig. 16.10** Gas volume to melt volume ratio  $\Psi$  for primary foaming of E-glass during ramp-heated at 5, 10, and 15°C/min as a function of (a) temperature and (b)  $\Phi^3 t^2$  where  $\Phi = dT/dt$  (eqn 16.14) with  $t = 0$  for  $T_0 = 1350^\circ\text{C}$  [58].

throughout the batch and melt in a manner similar to volcanic foam and solid glass foam produced for thermal insulation applications [119–131]. Hrma [58] also explained that “the decay of bulk foam tends to be more erratic than the decay of surface foam” by virtue of the fact that surface foam decays as bubbles burst at the top of the foams while bulk foam decays by bubble coalescence within the melt and eventually releases to the atmosphere.

**Effect of Redox State.** Laimböck [43] added carbon as a reducing agent, in the form of active carbon or graphite, to a soda-lime-silica batch refined with sulfate. First, the author observed that during the primary foaming process, more CO gas was generated at temperatures above 750°C than in oxidized melts. This was attributed to the oxidation of carbon by  $\text{CO}_2$  according to [43],



In addition, more CO was generated with active carbon than with graphite thanks to its extremely porous structure offering a large surface area for the above reaction. In practice,  $\text{CO}_2$  may react with carbon-containing components such as coke added to the batch or organic substances present in contaminated cullets [49].

Figure 16.11(a) shows the furnace temperature and the volume of foam per unit mass of batch as a function of time for oxidized and reduced soda-lime-silica glasses. The reduced batch contained 0.1 wt%  $\text{Fe}_2\text{O}_3$  and 0.2 wt% of either active carbon or graphite carbon. In all cases, 1 wt%  $\text{Na}_2\text{SO}_4$  was added to the batch and the atmosphere was dry nitrogen [43]. Note that the temperature rise was different from that imposed by Kim *et al.* [115]. Figure 16.11(a) shows that adding carbon to the batch, as a reducing agent, increases primary foaming but significantly decreases the maximum foam height and

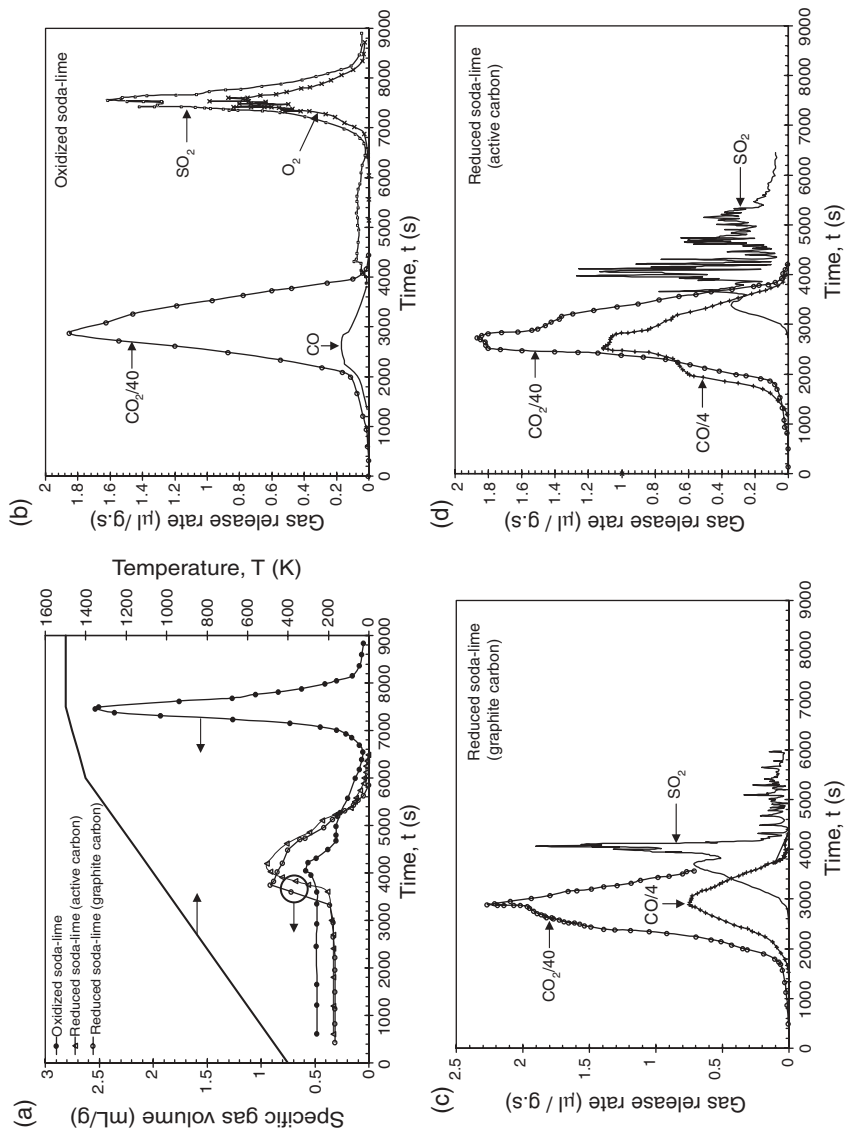
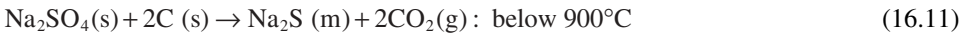


**Fig. 16.11** (a) Temperature ramp and specific gas volume and (b–d) gas release rate as a function of time for (b) oxidized soda-lime-silica, and reduced soda-lime-silica with 0.1 wt%  $\text{Fe}_2\text{O}_3$  and (c) 0.2 wt% of graphite carbon. In all cases, 1 wt%  $\text{Na}_2\text{SO}_4$  was added to the batch, the atmosphere was dry nitrogen, and the temperature was a function of time [43].

secondary foaming. In fact, adding a sufficient amount of carbon can entirely eliminate secondary foaming. Similar results were obtained by Faber *et al.* [46] for E-glass. This can be explained by considering the gas release rates during melting and fining.

Figure 16.11(b–d) shows the release rates of CO<sub>2</sub>, CO, SO<sub>2</sub> and O<sub>2</sub> for each batch as functions of time. It establishes that adding carbon lowered the temperature at which SO<sub>2</sub> production occurred and decreased sulfate retention in the glassmelt. This was also observed by Faber *et al.* [46] for E-glass. These observations were attributed to chemical reactions taking place at relatively low temperatures between carbon and sulfate SO<sub>4</sub><sup>2-</sup> to form sulfide (S<sup>2-</sup>), which at higher temperature reacts with sulfates to form SO<sub>2</sub> gas according to [55, 132]



Moreover, in sulfide rich soda-lime-silica melts depleted of sulfates consumed by the above chemical reactions caused by large addition of carbon to the batch, sulfur gas (S<sub>2</sub>) also evolves according to [43]



Overall, reducing the glass resulted in early consumption of sulfates, thus depleting the melt of refining agents. This, in turn, reduced the volume of refining gases (SO<sub>2</sub> and S<sub>2</sub>) produced during secondary foaming taking place at higher temperatures. Consequently, the smaller amounts of refining gases SO<sub>2</sub> and S<sub>2</sub> dissolved in the glassmelt may not be sufficient to cause supersaturation and bubble nucleation.

Moreover, primary foaming is affected by redox state and organic contamination of glass cullets. Using mixed (green, amber, and flint) cullets results in stronger primary foaming compared with clean cullets with a small variation in redox state [43]. In fact, the mismatch in redox state of mixed cullets causes sulfate (SO<sub>4</sub><sup>2-</sup>)/sulfide (S<sup>2-</sup>) reactions producing additional SO<sub>2</sub> [55] according to reaction (16.12). Finally, in sulfate-refined batches, organic contaminants present in the cullets react with CO<sub>2</sub> and SO<sub>4</sub><sup>2-</sup> to produce additional SO<sub>2</sub>, CO<sub>2</sub>, and CO according to reactions (16.10–16.12). These gases released at low temperature enhance primary foaming [43, 55].

Finally, foaming during nuclear waste vitrification in electric glass melters is not caused by the release of SO<sub>2</sub> gas. In fact, foaming in such systems is caused by the release of water vapor and O<sub>2</sub> from the oxidized melt [32, 34]. First, glasses used for vitrification are typically iron-alkali borosilicate glass rich in iron [32, 41]. Thus, oxygen gas is released at high temperatures during the reduction of polyvalent metal ions, mainly Fe<sub>2</sub>O<sub>3</sub>/FeO (reaction 16.1), but also manganese, cerium, or chromium [8, 32, 41]. Here also, reduced glasses were found to be less susceptible to foaming [32]. Carbon can be added as a reducing agent that reacts with Fe<sub>2</sub>O<sub>3</sub> at relatively low temperatures before oxygen gas can be trapped in the melt [41]. This was attributed to the lower content of dissolved O<sub>2</sub> in reduced glasses combined with the larger release of water vapor [32]. The latter decreases the melt viscosity [71, 83–85] and affects surface tension, resulting in less stable foams. These results were confirmed by Bickford *et al.* [34].

**Effect of Batch Grain Size, Compaction, and Culletts.** The size of the batch particles plays an important role in primary foam formation [70]. Using fine grains was found to reduce the foaming temperature and increase primary foaming during both ramp-heating and isothermal heating of soda-lime-silica glass with sulfate refining agent [74, 113, 114]. This was also observed with fiberglass [70]. The use of finer grains accelerates melting at the top of the batch, thereby sealing the batch and preventing gases generated at the bottom from escaping to the atmosphere [74]. By contrast, an increase in the particle size of the batch powder results in reduction of primary foaming [43]. Heating of coarse silica grains shifts the equilibrium of batch reactions towards higher temperatures compared with fine grains. At larger temperatures, the viscosity of the melt is significantly reduced, thereby easing the escape of gas bubbles to the atmosphere [74].

Similarly, using fine glass culletts (<1–2 mm) results in stronger primary foaming compared with coarse culletts [43]. Sintering of fine culletts occurs at much lower temperatures than for coarser grains, resulting in a viscous liquid layer covering the batch logs and preventing gas bubbles from escaping freely to the combustion space [43, 55]. By contrast, in coarse culletts, the gases generated at low temperatures escape through the pores between the culletts. Upon further heating, the gas released at higher temperatures can escape in bubbles rising to the surface thanks to the lower melt viscosity.

Finally, conditioning the batch material can significantly reduce foaming [72]. In fact, compacting the batch before melting leads to reduced primary foaming and increased foaming temperature. For example, Ahn and Hrma [72] showed that compacting and heat treating simulated nuclear waste batch above 1150°C prior to its introduction into the glass melting furnace limited significantly the extent of the primary foam. On the contrary, loose batch foams immediately upon contact with hot borosilicate melt [72]. In addition, the authors established that sintering of loose batch before introducing it on the glassmelt can delay foam formation. What is more, heat treatment of loose batch at high temperatures for several hours followed by sintering for less than one hour can completely prevent foaming [72].

**Effect of Batch and Glass Compositions.** The batch composition and that of the resulting melt have a strong effect on glass foaming mainly through their effects on the melt viscosity, redox state, and sulfate solubility [43]. For example, Cable *et al.* [75] as well as Kim and Hrma [114] found that the presence of  $\text{Al}_2\text{O}_3$  increased foaming of soda-lime-silica glass by decreasing the foaming temperature and stabilizing the glass foams. Retention of gases generated by batch melting was reduced by adding melting agents such as  $\text{Na}_2\text{NO}_3$  and by decreasing the amount of  $\text{SrCO}_3$  and  $\text{Al}_2\text{O}_3$  in the batch [74]. Finally, Laimböck [43] also showed that increasing the  $\text{Na}_2\text{O}$  content of soda-lime-silica glass or adding  $\text{Al}_2\text{O}_3$  while reducing  $\text{CaO}$  resulted in (i) an increase in foaming, (ii) a decrease in foaming temperature, and (iii) larger sulfate loss. This can be attributed to the following phenomena. First, adding small amounts of  $\text{SiO}_2$  and  $\text{Al}_2\text{O}_3$  or reducing the  $\text{Na}_2\text{O}$  and  $\text{CaO}$  content of soda-lime-silica glass significantly increases melt viscosity, which leads to more stable primary and secondary glass foams. Similarly, fluorine addition to fiberglass batch was found to reduce primary foaming due to the reduction in melt viscosity [70]. Second, increasing  $\text{SiO}_2$  or  $\text{Al}_2\text{O}_3$  content and/or decreasing  $\text{Na}_2\text{O}$  content reduces sulfate solubility in soda-lime-silica glass [133]. This in turn results in (i) lower foaming temperature, (ii) increased foam stability and height, and (iii) larger sulfate loss [43].

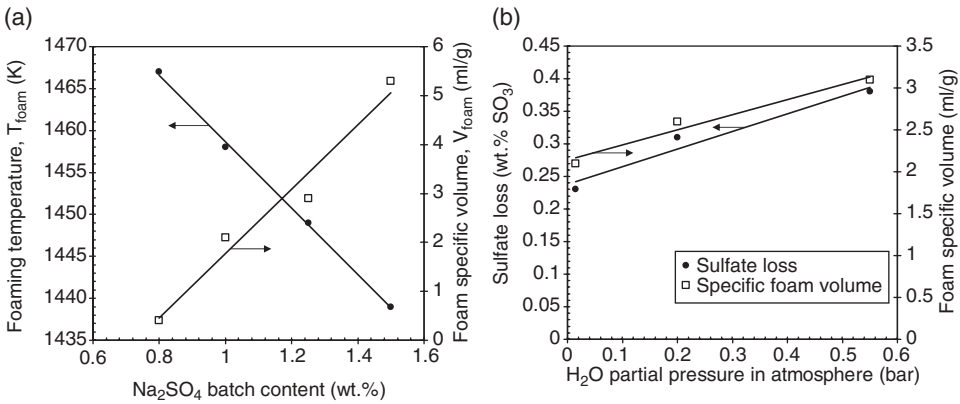


**Fig. 16.12** (a) Foaming temperature and foam specific volume as a function of mass fraction of  $\text{SO}_3$  added to soda-lime-silica glass melted in air at 1 atm. (b) Sulfate ( $\text{SO}_3$ ) loss and foam specific volume as a function of water vapor partial pressure in the atmosphere over the glassmelt. In all cases, the melt was made of soda-lime-silica glass with 1 wt%  $\text{Na}_2\text{SO}_4$  [43].

**Effect of Sulfate Addition.** Adding  $\text{Na}_2\text{SO}_4$  to the batch was found to (i) decrease significantly primary foaming (below  $1400^\circ\text{C}$ ) and (ii) increase secondary foaming (above  $1400^\circ\text{C}$ ) [20, 43]. Its decomposition caused mechanical stirring of the batch and accelerated the dissolution of sand grains [20, 43].

First, the reduction in primary foaming was attributed to the phase separation of sulfate from the glass, resulting in a sulfate gall also observed on single melt films of oxidized glass below  $1300^\circ\text{C}$ , as previously discussed [43]. Thus,  $\text{CO}_2$  bubbles tended to coalesce and the foam was less stable. Moreover, secondary foaming of mixed alkali and soda-lime silica was found to be stronger when water vapor and sulfate were present in the glassmelt [75, 77, 78]. In the absence of sulfate, secondary foaming of soda-lime-silica glass took place only in atmospheres containing oxygen [75]. The foaming temperature was also found to decrease with increasing sulfate addition to the batch as illustrated in Fig. 16.12(a). Adding sulfate to the batch resulted in stronger secondary foaming due to larger amounts of refining gases ( $\text{SO}_2$  and  $\text{O}_2$ ) generated during the sulfate thermal decomposition [43]. In addition, sulfur-containing oxidized glass melts are prone to secondary foaming due to decreasing  $\text{SO}_3$  solubility with increasing temperature [42] and dissolved oxygen concentration [134]. However, the amount of sulfate remaining in the glassmelt after refining was the same regardless of the initial sulfate concentration in the batch [43].

Finally, Faber *et al.* [46] proposed dissociating the oxidizing function of  $\text{Na}_2\text{SO}_4$  at low temperatures from its refining function at high temperature. To do so, they replaced 75% of the  $\text{Na}_2\text{SO}_4$  added to the batch of E-glass (0.05 wt% instead of 0.2 wt%) with oxidizing agents such as  $\text{NaNO}_3$ ,  $\text{MnO}_2$ ,  $\text{CaO}_2$ , and  $\text{NaBO}_3 \cdot \text{H}_2\text{O}$ . This ensured stable redox state while reducing the production of refining gases and therefore secondary foaming at high temperatures. They observed that adding these oxidizing agents (i) increased the foaming temperature, (ii) decreased the volume of  $\text{SO}_2$  released and the foam thickness, and

(iii) increased the residual  $\text{SO}_3$  content in the glass at  $1500^\circ\text{C}$ . They identified sodium perborate ( $\text{NaBO}_3 \cdot \text{H}_2\text{O}$ ) as having the strongest effect, followed by  $\text{CaO}_2$  and  $\text{NaNO}_3$ .

**Effect of Atmosphere Composition and Pressure.** The atmosphere composition is known to affect the stability of glass foams by virtue of the fact that gas species can influence (i) important physicochemical properties such as glassmelt viscosity and/or surface tension as well as (ii) sulfate chemistry, and (iii) melt redox state [49, 55]. It is generally believed that severe foaming in oxygen-fuel fired furnaces is caused by a higher partial pressure of water in the furnace atmosphere [49]. In fact, the atmosphere in oxygen-fired furnaces contains 40–60 vol.% of water vapor compared with 12–18 vol.% for air-fired furnaces.

First, water vapor has arguably the strongest effect on the physicochemical properties of glassmelts. For example, water dissolved in the glass reduces viscosity [83, 135] and therefore foam stability by enhancing foam drainage. Water also reduces surface tension, which tends to stabilize the foams [90]. Water can be introduced to the glassmelt entrapped in the batch minerals or due to batch moistening. It can also be introduced from the atmosphere by diffusion and/or convective mass transfer [136]. Laimböck [43] established that water vapor infiltrates the glassmelt preferably during melting of the batch and/or during foaming. In addition, water initially contained in the batch does not evaporate as easily when the water vapor partial pressure in the atmosphere is large, as encountered in the oxygen-fuel fired furnaces.

Laimböck [43] reported that wet atmosphere (i) increased foaming of soda-lime-silica glass refined with  $\text{Na}_2\text{SO}_4$ , (ii) reduced foaming temperature, and (iii) increased sulfate losses. This is illustrated in Fig. 16.12(b). He also observed that foaming in wet atmospheres lasted longer than in dry ones. This can be explained by the fact that as the amount of water dissolved in the glassmelt increases, the partial pressure of  $\text{H}_2\text{O}$  in bubbles also increases, thus diluting the fining gases in the bubbles and promoting further mass transfer of fining gases from the melt to the bubbles. This also shifts the equilibrium reaction (6) towards a more extensive decomposition of the sulfate refining agents. As a result, sulfate begins to decompose at a lower temperature resulting in lower sulfate retention. This mechanism was formulated as the “dilution model” [43]. This interpretation was confirmed by Kim *et al.* [115] for E-glass. However, Arkosiová *et al.* [57, 116] offered an alternative explanation by suggesting that water reacted with sulfate ( $\text{SO}_4^{2-}$ ), sulfite ( $\text{SO}_3^{2-}$ ), and sulfide ( $\text{S}^{2-}$ ) to produce  $\text{O}_2$ ,  $\text{SO}_2$ , and even  $\text{H}_2\text{S}$  in reduced soda-lime-silica glass refined with sulfate and containing carbon in the form of coke. Overall, water in the furnace atmosphere helps the refining action of the sulfate, making it possible to lower the addition of sulfate to obtain an equally efficient refining process compared to dry atmosphere.

Moreover, Fig. 16.13 shows the gas volume  $V_{\text{gas}}$  to melt volume  $V_{\text{melt}}$  ratio  $\Psi (= V_{\text{gas}}/V_{\text{melt}})$  as a function of temperature for primary foaming of E-glass containing sulfates during ramp-heating at  $5^\circ\text{C}/\text{min}$  under dry or wet air and dry or wet carbon dioxide atmospheres [115]. It is evident that the presence of water vapor in the atmosphere reduced the foaming temperature and the amount of gas entrapped in the glass foam. Similar results were obtained by Cable and co-workers [77, 78] for binary silicate melts. The authors also found that soda-lime-silica and alkali-silica glass foaming was stronger in pure oxygen atmosphere. Kappel *et al.* [71] also showed that humidity in the atmosphere destabilized the foams made of various glasses. This apparent contradiction with results reported by Laimböck [43] (Fig. 16.12b) can be explained by the dilution effect of water vapor during the batch melting process, which

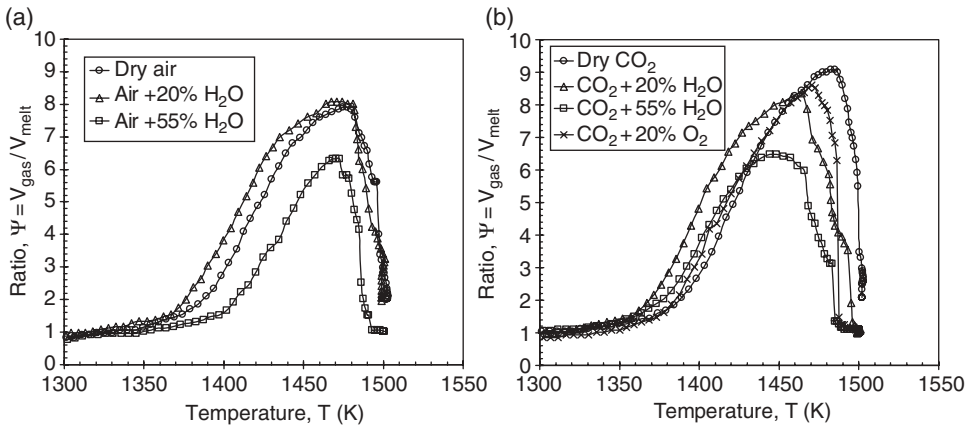


**Fig. 16.13** Gas volume to melt volume ratio for primary foaming of E-glass containing sulfates during ramp-heating at 5°C/min under (a) dry and wet air and (b) dry and wet carbon dioxide atmosphere [115].

enhanced sulfate losses at temperature below 1250°C. This effect was enhanced by the facts that (i) significantly less sulfate was added to the E-glass batch (0.17 wt%) [115] compared with the soda-lime batch (0.55 wt%) [43], and (ii) the amount of batch used by Laimböck [43] (~150 g) was much larger than that used by Kim *et al.* [115] (4–5 g).

Furthermore, reducing atmosphere in contact with glass foam tends to destabilize it, if not destroy it [43, 75, 79]. In industrial furnaces, reducing atmosphere is achieved by firing with an excess of fuel (reducing firing) as opposed to an excess of air or oxygen (oxidizing firing) [43]. For example, Cooper and Kitchener [79] reviewed the fact that foam made of molten silicate slags was more prevalent in oil-fired furnaces, which usually burn with excess air (i.e., oxidizing). However, it was rarely observed in reducing atmospheres such as so-called “coke-oven gas” consisting of H<sub>2</sub>, CH<sub>4</sub>, N<sub>2</sub>, and CO, and so-called “producer gas” consisting of a H<sub>2</sub>, N<sub>2</sub>, and CO. Reducing atmospheres used experimentally have included (i) N<sub>2</sub> [78], and mixtures of (ii) N<sub>2</sub> and CO [43] or (iii) N<sub>2</sub> and H<sub>2</sub> [75], for example. Laimböck [43] showed that primary foam made of oxidized soda-lime-silica glass decayed dramatically as soon as a mixture of CO in N<sub>2</sub> was introduced in the furnace. The effect was stronger as the concentration of CO increased from 0.1 to 1.0 wt%. The author suggested that a minimum content of CO in the atmosphere should be reached in order to reproduce this effect in industrial furnaces [43]. In addition, the polyhedral bubbles at the top of the foam were found to be extremely sensitive and collapsed in contact with reducing atmosphere [43]. Similarly, Cable and co-workers [75, 77, 78] showed that binary glasses did not foam in a pure N<sub>2</sub> or a N<sub>2</sub>-H<sub>2</sub> mixed atmosphere. In addition, increasing the partial pressure of SO<sub>2</sub> in the atmosphere destabilized foams made from various glass batches [71, 78] due to the fact that SO<sub>2</sub> causes the glassmelt viscosity to decrease significantly.

Finally, a decrease in pressure of the surrounding atmosphere reduces the mass of gas retained in the batch and in the glassmelt. It lowers the temperature at which carbon dioxide is generated in the batch and thus promotes primary foaming [74]. It also decreases the solubility of SO<sub>2</sub>, H<sub>2</sub>O, and O<sub>2</sub> and favors secondary foaming as observed in reduced-pressure refining [69].

### 16.4.3 Steady-state Glass Foaming by Gas Injection

#### 16.4.3.1 *Experimental Apparatus and Procedure*

Figure 16.8b schematically shows the interior of a furnace used to study steady-state glass foams. In this method, an arbitrary gas mixture is continuously injected within the molten glass contained in a transparent crucible placed in a furnace at constant temperature. Here, bubbles are not generated by chemical reactions but instead injected in the glassmelt through a Pt capillary. The gas inside the bubble can be different from that in the furnace atmosphere. For example, van der Schaaf and Beerkens [117] injected  $N_2$  and  $CO_2$  bubbles in molten soda-lime-silica glass at temperatures between 1300 and 1400°C in air atmosphere. This method produces a steady foam layer with constant height after a rapid growth phase [43]. It can also be used to analyze foam decay by simply stopping the gas supply [117].

#### 16.4.3.2 *Experimental Observations and Foaming Regimes*

Experimental observations indicate that glass foams produced by gas injection do not form for any arbitrarily small gas flow rate. To scale for the container cross-section, the superficial gas velocity  $j$  is defined as the volumetric gas flow rate  $Q_g$  (in m<sup>3</sup>/s) divided by the cross-sectional area of the container denoted by  $A$  (in m<sup>2</sup>) so that  $j = Q_g / A$  (in m/s) [137]. A minimum superficial gas velocity  $j_m$  should be reached to initiate foaming when injecting air bubbles in molten glass [39, 43]. The same observations have been made for various aqueous solutions [138–143] as well as for slag foaming [144–150]. The onset of foaming corresponds to the situation when bubbly flow coexists with only a single layer of closely packed bubbles accumulating at the free surface. Three different foaming regimes have been identified [39]:

- If  $j < j_m$ , the gas flux  $j$  reaching the liquid surface is not sufficient to create a stable foam layer (Fig. 16.14a). If  $j = j_m$ , the foam layer consists of a monolayer of bubbles whose thickness is  $2r_0$  where  $r_0$  is the average radius of the bubbles (Fig. 14b).
- If  $j_m < j \leq j_{cr}$ , the foam reaches a steady state and its thickness increases as the gas influx increases (Fig. 16.14c) [39].
- If  $j \geq j_{cr}$ , the excess of mass flux over the critical superficial gas velocity  $j_{cr}$  cannot be released at the top of the foam and has to be stored within the foam. Thus, the foam volume grows continuously until all available liquid is dispersed in the foam, so a steady state is never reached [39]. Beyond a certain mass flux, vent holes may start developing within the foam, which stops growing or may even start decaying [138, 151].

Note that the last regime is not shown in Fig. 16.14 as the foam looks very similar to that shown in Fig. 16.14(c) except that bubbles may be bigger and the foam thicker with large pockets of air and possible vents. Note also that in glass melting furnaces this regime is less likely to be observed since the foam is not confined. Instead, foam is more likely to flow and spread horizontally over the glassmelt surface [152, 153].

#### 16.4.3.3 *Onset of Glass Foaming*

Figure 16.15 shows the steady-state foam thickness  $H_1$  as a function of superficial gas velocity  $j$  measured by bubbling air in sulfate-free molten soda-lime-silica glass at different temperatures [43]. It illustrates the existence of a minimum superficial gas velocity for onset of foaming  $j_m$  which can be determined by extrapolating the linear curve fit to the limiting case when  $H_\infty = 0.0$ .

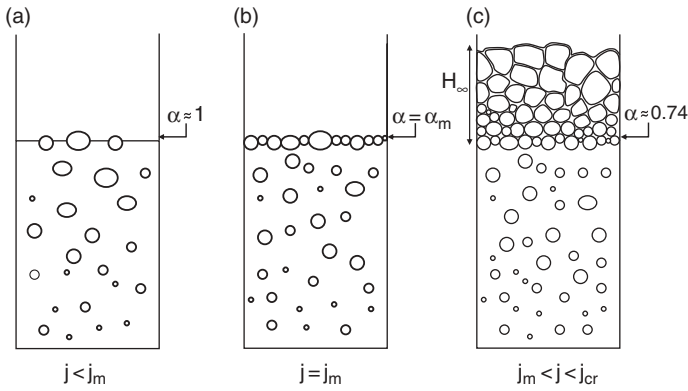


**Fig. 16.14** Schematic of the behavior of a foaming solution as the superficial gas velocity increases (a) bubbly flow without foam, (b) onset of foaming, (c) developed foam layer.

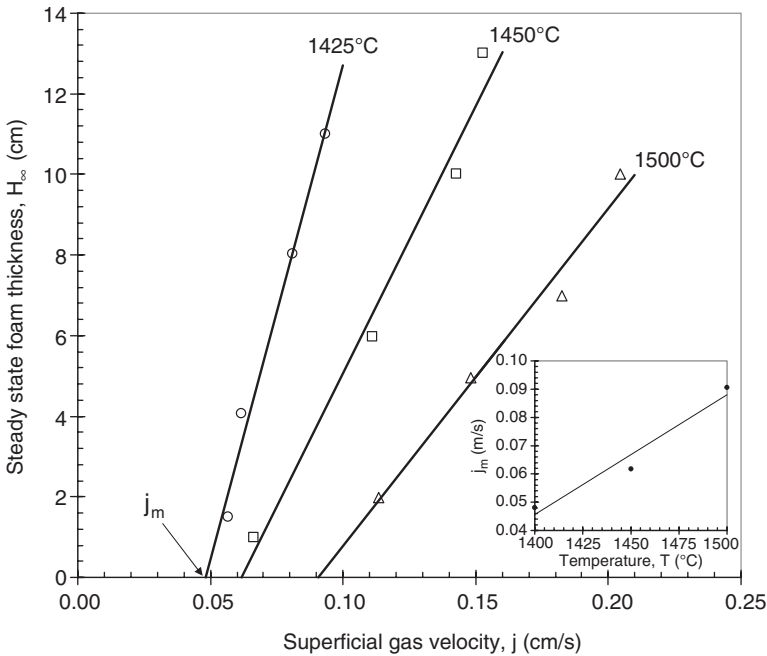


**Fig. 16.15** Steady state foam thickness v. superficial air velocity for sulfate-free soda-lime-silica glass (75 SiO<sub>2</sub>-15 NaO<sub>2</sub>-10 CaO, wt%) at different temperatures [43].

#### 16.4.3.4 Steady-state Foam Thickness

**Effect of Temperature.** The stability and steady-state thickness of glass foams decrease with increasing temperature [43, 79]. This is illustrated in Fig. 16.15 where, for a given superficial gas velocity  $j$  larger than  $j_m$ , the foam thickness decreases with increasing

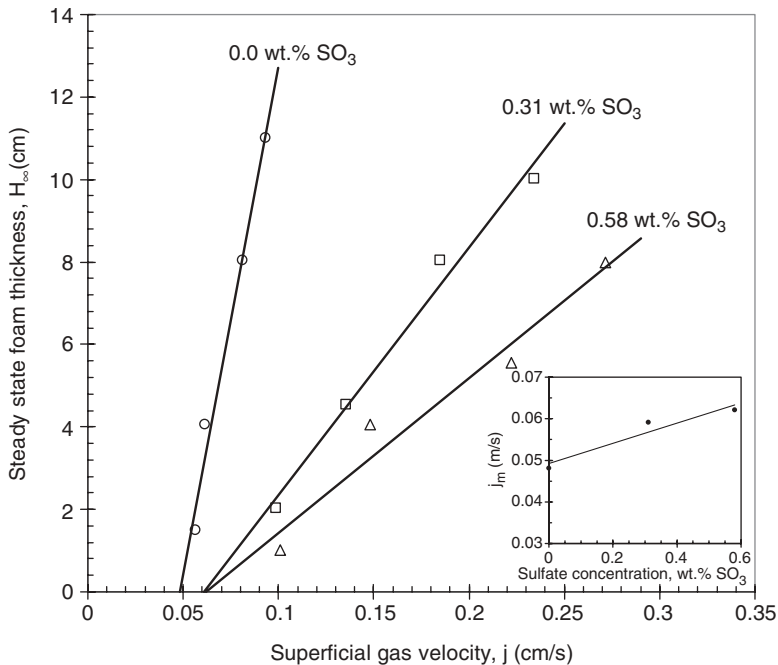


**Fig. 16.16** Steady state foam thickness v. superficial argon velocity for soda-lime-silica glass with different initial sulfate content at 1425°C [43].

temperature. This can be attributed to the fact that the melt viscosity decreases as the temperature increases, resulting in shorter drainage time. For the same reasons, the inset in Fig. 16.15 shows that  $j_m$  increases as the temperature increases, which makes the bubbles less stable, requiring larger flow rates for onset of foaming.

**Effect of Sulfate Addition.** Figure 16.16 shows the steady-state foam thickness as a function of superficial gas velocity reported by Laimböck [43] for soda-lime-silica glass with different initial  $\text{SO}_3$  content. The foam was generated by injecting argon into the glassmelt at 1425°C [43]. First, the inset of Fig. 16.16 indicates that  $j_m$  increases as sulfate concentration increases. In addition, the foam tended to be less stable for larger sulfate content. This can be attributed to the decrease of viscosity caused by the presence of sulfate [43]. Note that here only the effect of sulfates on the thermophysical properties of the glassmelt and their impact on foaming were assessed.

## 16.5 Modeling

### 16.5.1 Introduction

In order to design, optimize, and operate industrial glass melting furnaces and to mitigate the negative effects of glass foaming, it is necessary to develop physical models informed by experimental observations and accounting for the most important physical phenomena.

Models reported in the literature can be divided into two categories: (i) time-dependent models predicting foam growth and decay; and (ii) steady-state models predicting the onset of foaming and the steady-state foam thickness. Note that most models presented and developed for glass foams can typically be used for foams made of other viscous fluids.

## 16.5.2 Dynamic Foam Growth and Decay

### 16.5.2.1 Foaming by Thermal Decomposition

Kappel *et al.* [71] showed experimentally that the thickness of glass foams generated from soda-lime-silica, E-glass, borosilicate, and brown glasses systematically decayed exponentially during foam collapse and could be expressed as  $H(t) = H_0 \exp(-k_s t)$  where  $H_0$  is the initial foam thickness. The empirical constant  $k_s$  was a function of (i) temperature, (ii) glassmelt properties (e.g., density, surface tension, viscosity), and (iii) partial pressures of  $H_2O$  and  $SO_2$  in the furnace atmosphere. However, the authors did not provide a relationship between  $k_s$  and all these parameters. Moreover, they reported that  $k_s$  was approximately equal to  $20k_L$  reported for the vertical film thickness as previously discussed.

Recently, Hrma [58] proposed a model for foaming caused by  $SO_2$  and  $O_2$  release during sulfate thermal decomposition in E-glass between 1335 and 1440°C. The author expressed the gas to melt volume ratio  $\Psi(t)$  as a function of time as

$$\Psi(t) = \frac{V_{gas}}{V_{melt}} = \Psi_0(1 + b\Phi^3 t^2) \quad (16.14)$$

where  $\Phi = dT/dt$  is the heating rate while  $b$  and  $\Psi_0$  are empirical parameters determined from experimental data. The time  $t = 0$ s was set for temperature  $T_0 = 1335^\circ\text{C}$  so that  $T = T_0 + \Phi t$ . This model successfully predicted the behavior of glass foam made of E-glass batch subjected to heating rates of 5, 10, and  $15^\circ\text{C}/\text{min}$  beyond  $T_0$  as reported by Kim *et al.* [115]. Figure 16.10(b) plots  $\Psi(t)$  versus  $\Phi^3 t^2$  and illustrates how the experimental data shown in Fig. 10(a) for different heating rates collapse on a single line during the exponential growth phase as predicted by eqn (16.14) with  $b = 5.39 \times 10^{-3} \text{ s}/\text{K}^3$  and  $\Psi_0 = 0.587$ .

### 16.5.2.2 Foaming by Gas Injection

Pilon *et al.* [154] presented an experimentally validated model to analyze the transient formation of a foam layer produced by injecting gas bubbles in a foaming solution. Their model was based on the mass conservation equation for the gas phase in the foam combined with models for the average foam porosity. The authors assumed that, during the growth phase ( $t \leq \tau_{bf}$ ), no gas escapes at the top of the foam via bubble bursting. Then, the foam thickness can be expressed as [154]

$$H(t) = \frac{j t}{\bar{\phi}} \text{ for } t \leq \tau_{bf} \quad (16.15)$$

where  $j$  is the incoming superficial gas velocity at the bottom of the foam while  $\bar{\phi}$  is the average foam porosity. The latter can be taken as constant and equal to  $\bar{\phi} = 0.82$  for practical calculations [154]. The time constant  $\tau_{bf}$  corresponds to the characteristic lifetime

of a lamella at the top of the foam. The model predictions showed very good agreement with experimental data for aqueous solutions with 10% glycerine + 80mg/l of Marlophen-89 [138] for low superficial gas velocity. It can also provide an upper limit of the foam thickness for intermediate and large superficial gas velocities.

More recently, Van der Schaaf and Beerkens [117] developed a dynamic model for the growth and decay of glass foams. The authors assumed that foam was made of superimposed layers of monodisperse hemispherical shells. The mass conservation equation for the gas phase in the foam was given by [117]

$$\frac{dH}{dt} = j(t) - j(t - \tau_{bf}) \quad (16.16)$$

where  $j(t)$  is the superficial gas velocity for bubble entering the foam layer at the bottom and  $j(t - \tau_{bf})$  is the superficial gas velocity leaving the foam due to the bursting of bubbles at the top of the foam after spending an average lifetime  $\tau_{bf}$ . The average lifetime  $\tau_{bf}$  of a bubble at the top of the foam was estimated by solving mass and momentum conservation equations for the molten glass draining in the lamella of an hemispherical shell. The fluid was treated as non-compressible and Newtonian and the interfaces were assumed to be (i) fully mobile, (ii) partially mobile, or (iii) fully immobile. An expression for the average bubble lifetime was derived for each boundary conditions as a function of density  $\rho$ , viscosity  $\mu$ , and average bubble radius  $r_0$  and given by [117]

$$\tau_{bf} = \frac{\mu}{3\rho gr_0} \left[ \ln \left( \frac{\delta_0}{\delta_c} \right) + 2 \frac{\psi r_0^2}{\mu / \delta_c} \right] \quad (16.17)$$

where  $\delta_0$  is the initial lamella thickness,  $\psi$  is a parameter ranging from 0 to infinity corresponding to the limit cases of fully mobile and fully immobile bubble interface, respectively. The critical lamella thickness  $\delta_c$  was taken to be 100nm based on empirical observations [43, 71]. The advantage of this model is that it can predict both the growth and the decay of foam. The expression for  $\tau_{bf}$  was in good agreement with those derived by Pilon *et al.* [154] by considering the intersection of their transient foam model [154] given by eqn (16.15) and the semi-empirical steady-state model [155] discussed in the following section (eqn 16.28).

The model was solved in a discontinuous manner in terms of time. Its predictions were compared with experimental data for foam made by injecting either  $N_2$  or  $CO_2$  in soda-lime-silica glass at 1300 and 1400°C [117]. The resulting foam porosity was 91% and the average bubble radius varied from 5 to 8.3mm as the gas flow rate increased. Good agreement was observed between model predictions and experimental data for  $\psi$  equal to 2.5/m. However, it remains unclear how this value of  $\psi$  was obtained and what value of  $\delta_0$  was used to achieve these results.

For constant superficial gas velocity  $j$ , the model developed by Van der Schaaf and Beerkens [117] predicts the foam height as

$$H(t) = jt \text{ for } t \leq \tau_{bf} \quad (16.18)$$

$$H_{\infty} = j\tau_{bf} \text{ for } t > \tau_{bf} \quad (16.19)$$

where  $H_{\infty}$  denotes the steady-state foam thickness. Note that eqn (16.18) ignores the contribution of the liquid to the overall foam thickness, unlike the transient model given by eqn (16.15) [154], i.e., it assumes  $\bar{\phi} = 1.0$ . In addition, eqn (16.19) corresponds to the concept of unit of foaminess introduced by Bikerman [137]. However, the validity of this concept has been questioned extensively in the literature, as discussed in detail in the next section [39, 155–158]. Finally, eqn (16.19) predicts that foam forms for any superficial gas velocity, which contradicts the concept of the onset of foaming introduced by Hrma [39] and illustrated in Figs 16.15 and 16.16.

### 16.5.3 Steady-state Glass Foams

Based on experimental observations previously reviewed, steady-state foams are characterized by the minimum superficial gas velocity for onset of foaming  $j_m$  and by their thickness  $H_{\infty}$ . The following sections discuss models associated with both of these parameters.

#### 16.5.3.1 Onset of Foaming

Pilon and Viskanta [159] argued that coalescence of rising bubbles with bubbles at rest at the liquid free surface was the main physical phenomenon controlling the onset of foaming. The authors used the drift flux model [160] to derive the following expression for  $j_m$  as a function of the maximum void fraction for onset of foaming  $\alpha_m$ , operating conditions, and physico-chemical properties of the two phases,

$$j_m = v_{\infty} f(r^*) \alpha_m (1 - \alpha_m)^{n-1} \quad (16.20)$$

where  $f(r^*)$  is a function of the dimensionless bubble radius  $r^*$ . Both depend on the thermophysical properties of the melt and on whether the two-phase flow regime in the liquid below the foam was viscous, distorted bubble, and churn-turbulent as summarized in Table 16.1 of ref. [159]. Figure 16.17 compares the experimental data for the minimum superficial gas velocity for onset of foaming  $j_m$  with the model predictions given by eqn (16.20), using a maximum void fraction  $\alpha_m = 0.85$  corresponding to the case of small probability of coalescence ( $P < 66\%$ ) between a rising bubble and a bubble at rest at the liquid free surface. Relatively good agreement was found between model predictions and experimental data for a wide range of  $j_m$  values and various viscous fluids (e.g., slags, glass, glycerol) [159].

#### 16.5.3.2 Steady-state Foam Thickness

**Foaming Index and Related Models.** The first model predicting the steady-state foam height as a function of superficial gas velocity  $j$  was proposed by Bikerman [137]. He suggested that below the critical superficial gas velocity  $j_{cr}$ , the steady-state foam thickness  $H_{\infty}$  increases linearly with superficial gas velocity [137],

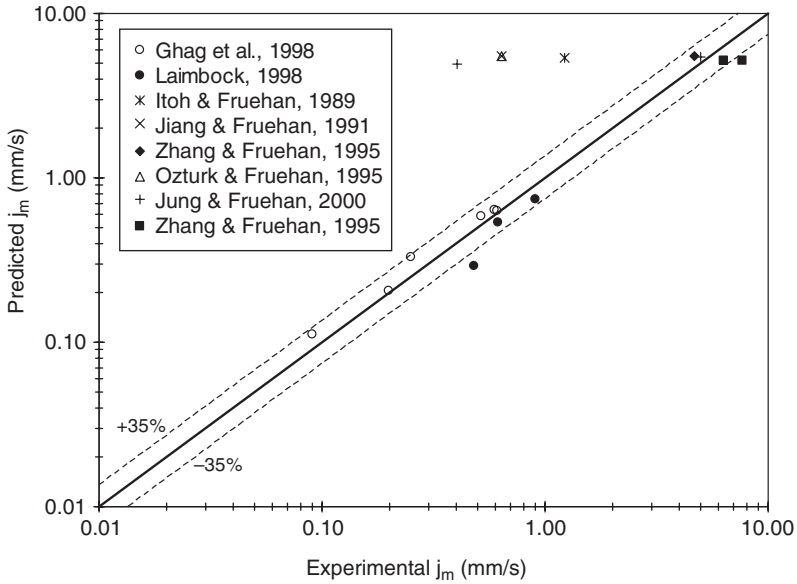


**Fig. 16.17** Comparison between experimental and predicted minimum superficial gas velocity for onset of foaming for viscosity dominated drainage associated with a probability of bubble coalescence less than 66% [159].

$$H_{\infty} = \Omega j \quad \text{if } j \leq j_{cr} \quad (16.21)$$

where  $\Omega$  is a constant called the “unit of foaminess” or “foaming index.” It was considered to be a physical characteristic of the liquid corresponding to the average residence time of a bubble in the foam [44, 117], i.e.,  $\Omega = \tau_{bf}$ . Beyond the critical mass flux  $j_{cr}$ , the entrainment of the liquid into the foam by rising bubbles cannot be balanced by drainage and the foam thickness increases without limit. However, experimental data for viscous oils [39, 157] indicate that the transition from a steady-state foam to a constantly growing foam is not abrupt at  $j = j_{cr}$  but continuous, thereby indicating that  $\Omega$  is not a fluid property but increases as the mass flux  $j$  increases. Lin and Guthrie [158] confirmed the validity of eqn (18.21) for small superficial gas velocity. However, the foam tended to become unstable with decreasing steady-state thickness as the superficial gas velocity increased.

Jeelani *et al.* [138] proposed a model for the steady-state foam thickness accounting for binary bubble coalescence taking place within the foam. The steady-state foam thickness was expressed as a function of the thermophysical properties of the liquid phase, the binary coalescence time, and the average foam porosity. The binary coalescence time as well as the average foam porosity were determined experimentally from the measurements of the average bubble diameter as a function of depth of foam made of nitrogen bubbles in water with 10% glycerinate Marlophen 89 and 812 [138]. Good agreement was found between the model predictions and the experimental data. Unfortunately, most of the other experimental

studies of steady-state foam thickness did not provide the variation of the average bubble diameter along the foam height. Also, neither the binary coalescence time nor the average foam porosity could be determined, making the model validation impossible for other solutions [155].

A series of studies on slag foams in iron and steelmaking processes was carried out by Fruehan and co-workers to correlate the foaming index with slag properties and bubble size [144–148, 150, 161]. All the experiments consisted of bubbling argon in a cylindrical tank containing liquid slag with various amounts of CaO, SiO<sub>2</sub>, FeO, MgO, and Al<sub>2</sub>O<sub>3</sub> at high temperatures. Zhang and Fruehan [147] performed a dimensionless analysis using the Buckingham–Pi theorem to relate the unit of foaminess  $\Omega$ , liquid viscosity  $\mu$ , density  $\rho$ , surface tension  $\sigma$ , and average bubble diameter  $D_0$ . Three dimensionless groups were identified and related by a power-type of law. Experimental data for CaO-SiO<sub>2</sub>-FeO-MgO-Al<sub>2</sub>O<sub>3</sub> suggested the following semi-empirical expression for the unit of foaminess  $\Omega$  [147]:

$$\Omega = 115 \frac{\mu^{1.2}}{\sigma^{0.2} \rho D_0^{0.9}} \quad (16.22)$$

This semi-empirical model was based on experimental data obtained for similar slag compositions, thermophysical properties, and average bubble diameter, making this model valid for a very narrow range of fluids and operating conditions. In fact, Ghag *et al.* [140] studied pneumatic foams formed by bubbling nitrogen in different viscous solutions containing water, glycerinate (78 to 95 vol.%), and SDBS surfactant. The authors showed that “there was a poor correlation” between their experimental data and eqn (16.22). Experimental results indicated that the foaming index predicted by eqn (16.22) should be more sensitive to changes in surface tension and that the exponent associated with the average bubble diameter  $D_0$  was a major cause of discrepancies. From these observations, Ghag *et al.* [162, 163] also developed a model for the unit of foaminess  $\Omega$  using the Buckingham–Pi theorem. They performed the same analysis as that by Zhang and Fruehan [147] but replaced the equilibrium surface tension by the effective elasticity of liquid films  $E_{eff}$  for solutions following Langmuir behavior to yield [140]

$$\Omega = 1.0 \times 10^6 \frac{(\rho g)^2 D_0^3}{\mu E_{eff}} \quad (16.23)$$

Unfortunately,  $E_{eff}$  is not always available and its measurements may be tedious [140]. Thus, validation of the model for a wide range of experimental conditions and fluid has not been performed.

Finally, Beerkens and Van der Schaaf [44] combined the above described model given by eqns (16.17) and (16.19) with a model predicting the gas generation rate during fining to predict the steady-state foam thickness. The authors developed a thermochemical model to estimate the volume of gases released during refining of glassmelt and accounting for the temperature, composition, and redox state of the glassmelt along with sulfate decomposition and other redox reactions involving various gas species (e.g., SO<sub>2</sub>, O<sub>2</sub>, N<sub>2</sub>, CO<sub>2</sub>). Their model assumed thermodynamic equilibrium between the melt and the gas phases. It

enabled the prediction of  $j$  as a function of temperature necessary to predict the foam thickness and foaming temperature.

**Hrma's Model.** Hrma [39] developed a model for a steady-state foam blanket that did not use the concept of foaming index or the Buckingham–Pi theorem. Instead, the steady-state foam thickness was described in terms of the two previously discussed limiting gas fluxes  $j_m$  and  $j_{cr}$  according to [39]

$$H_\infty = 2r_0 + 2r_0 b_h \left[ \frac{1/j_m - 1/j_{cr}}{1/j - 1/j_{cr}} - 1 \right] \quad (16.24)$$

where  $r_0$  is the average radius of bubbles in the foam, and  $b_h$  is a constant depending on the gravitational drainage and on the survival time of a critically thin film separating the foam from the atmosphere.

Hrma [39] suggested that eqn (16.21) proposed by Bikerman [137] is only valid (i) for evanescent foams for which the liquid lamellae separating the bubbles in the foam rupture as soon as the critical thickness of the foam is reached, and (ii) for very small superficial gas velocity (i.e.,  $j \ll j_{cr}$ ). In that case, eqns (16.21) and (16.24) are equivalent as long as  $b_h = 1$  and  $\Omega \approx 2r_0/j_m$ . In addition, for foams characterized by similar superficial gas velocities  $j_m$  and  $j_{cr}$ , only a narrow range of superficial gas velocity  $j$  can generate a steady-state foam. This might have been the case observed by Watkins [151].

Finally, Hrma's model [39] provides insights into the mechanism of foam formation and stability by qualitatively explaining reported experimental data. Unfortunately, it lacks expressions for  $j_{cr}$  and  $b_h$ . However, the expression for  $j_m$  given by eqn (16.20) could be used in eqn (16.24).

**Dimensional Analysis of Foam Thickness Governing Equation.** More recently, Pilon and co-workers [155, 164] developed a general correlation capable of predicting the steady-state foam thickness for a variety of systems having widely different thermophysical properties and average bubble diameters. Instead of using the Buckingham–Pi theorem, the mass and momentum conservation equations for the liquid phase derived by Bhakta and Ruckenstein [82] were adapted to derive the governing equation for the steady-state foam thickness  $H_\infty$ . The authors assumed that (i) the foam consisted of dodecahedron bubbles of the same size, (ii) the Plateau borders were randomly oriented, (iii) the drainage through the Plateau borders due to film thinning was negligible compared to that due to gravity (see [82, 165] for additional discussion), (iv) coalescence of bubbles and Ostwald ripening within the foam were absent, (v) surface tension was constant, (vi) the container wall effects were negligible, and (vii) the temperature was constant and uniform throughout the foam. This governing equation was then scaled by dimensional analysis based on physical arguments to obtain the following two dimensionless numbers  $\Pi_1$  and  $\Pi_2$  [155]:

$$\Pi_1 = \frac{\rho g r_0^2}{\mu(j - j_m)} \quad \text{and} \quad \Pi_2 = \frac{\mu(j - j_m)}{\sigma} \times \frac{H_\infty}{r_0} \quad (16.25)$$

The number  $\Pi_1$  can be interpreted as the ratio of the gravitational force to the viscous force on an average bubble of radius  $r_0$  having a velocity  $(j - j_m)$ . Similarly,  $\Pi_2$  corresponds to the ratio of the viscous force to the surface tension force times the ratio of the steady-state

foam thickness to the average bubble radius. Both  $\Pi_1$  and  $\Pi_2$  can be expressed as functions of well known dimensionless numbers [155]:

$$\Pi_1 = \frac{Re}{Fr} \text{ and } \Pi_2 = Ca \left( \frac{H_\infty}{r_0} \right) \quad (16.26)$$

where  $Re$ ,  $Fr$ , and  $Ca$  are the Reynolds, Froude, and Capillary numbers, respectively, defined as,

$$Re = \frac{\rho_c(j - j_m)r_0}{\mu}, \quad Fr = \frac{(j - j_m)^2}{gr_0}, \quad Ca = \frac{\mu(j - j_m)}{\sigma} \quad (16.27)$$

The relationship between  $\Pi_1$  and  $\Pi_2$  was assumed to follow a power-law, i.e.,  $\Pi_2 = K\Pi_1^n$  where  $K$  and  $n$  were constant parameters determined from experimental data. More than 120 experimental data points for foams formed from high viscosity liquids and various gases and injection methods were considered [43, 140, 144–150, 161]. The superficial gas velocity for onset of foaming  $j_m$  can be determined either by eqn (16.20) or from experimental data assuming a linear relationship between  $H_\infty$  and  $j$  as illustrated in Figs 16.15 and 16.16. The ranges of thermophysical properties and experimental conditions were the following: (i)  $46 \text{ mPa}\cdot\text{s} < \mu < 12,100 \text{ mPa}\cdot\text{s}$ , (ii)  $1,200 \text{ kg/m}^3 \leq \rho \leq 3,000 \text{ kg/m}^3$ , (iii)  $69.5 \text{ mN/m} \leq \sigma \leq 478 \text{ mN/m}$ , (iv)  $0 \leq j \leq 40 \text{ mm/s}$ , and (v)  $0.7 \text{ mm} \leq r_0 \leq 20 \text{ mm}$  [155]. The corresponding dimensionless parameters  $\Pi_1$  and  $\Pi_2$  cover the range from 80 to 5030 and from  $5 \times 10^{-4}$  to 0.76, respectively. Figure 16.18 shows the relationship between the

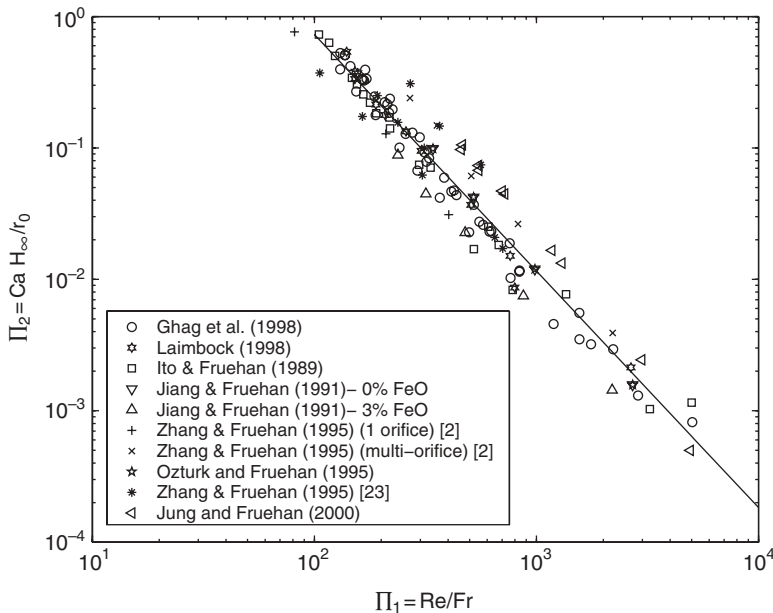


**Fig. 16.18** Correlation of dimensionless numbers  $\Pi_2$  v.  $\Pi_1$  for foams made from a wide range of viscous liquids.

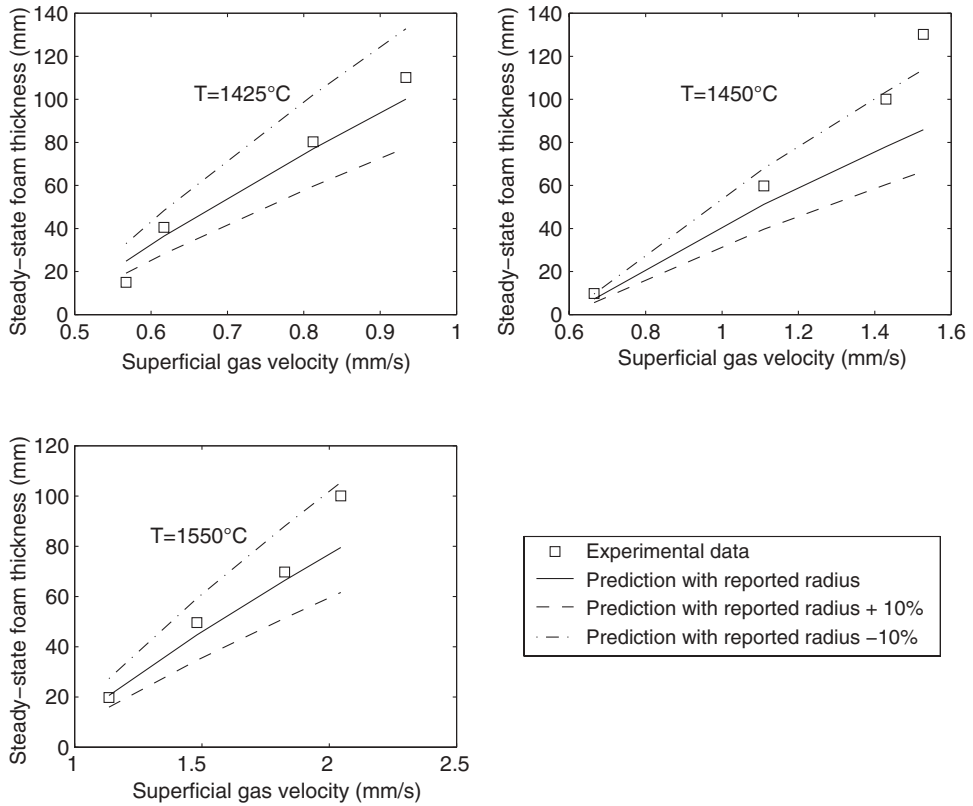


**Fig. 16.19** Influence of the bubble radius on the model predictions and comparison with experimental data for glass foams made by injecting air into sulfate free soda-lime-silica melt at 1425, 1450, and 1550°C [43].

dimensionless parameters  $\Pi_1$  and  $\Pi_2$  with  $K = 2905$  and  $n = -1.80$ . The following relationship between the physically relevant dimensionless numbers can be written as

$$\frac{H_\infty}{r_0} = \frac{2905}{Ca} \left( \frac{Fr}{Re} \right)^{1.80} \tag{16.28}$$

Figure 16.19 compares the steady-state foam thickness measured experimentally with predictions by eqn (16.28) using the reported radius  $r_0$  and the reported radius with  $\pm 10\%$  deviation. The foam was made by injecting air in sulfate-free soda-lime-silica glass at different temperatures (see Fig. 16.15) [43]. The predictions vary significantly depending on the average bubble radius  $r_0$  used and, in this particular case, the experimental data lie within the prediction range. In general, predictions of  $H_\infty$  by eqn (16.28) fell within 35% of experimental data. This is quite acceptable given the wide bubble size distribution and the uncertainty in the experimental data and the thermophysical properties.

Moreover, Lotun and Pilon [164] applied the Buckingham–Pi theorem based on six independent variables ( $\mu, \rho, \sigma, j - j_m, H_\infty, r_0$ ) but did not use the concept of foaming index. Their analysis resulted in four dimensionless numbers, namely  $Fr, Re, Ca,$  and  $H_\infty/r_0$ , given by eqn (16.27). Their final power-law correlation was in excellent agreement with that derived by Pilon *et al.* [155] and given by eqn (16.28).

#### 16.5.4 Experiments and Model Limitations

It should be noted that all previously discussed experimental results and associated models were obtained in laboratory crucibles; thus, one should be careful in extending these results to glass foams in industrial glass melting furnaces [74]. Some of the more important effects that are difficult to observe or reproduce in small-scale laboratory systems are as follows:

1. The refining reactions observed in crucibles at high temperature would most probably occur only at the top of the batch in the actual furnace that is directly exposed to radiant heating, whereas the center of the batch is too cold for initiation of fusion reactions due to the “insulation effect” of the expanded batch.
2. Partition of the gas generated in the batch between what is released (escaped) to the combustion space and what is entrapped in the form of gas bubbles in the glassmelt and then carried away by the convection currents is difficult if not impossible to study in laboratory systems since convection currents encountered in glass melting tanks cannot be reproduced in small crucibles.
3. Volatilization of glass volatile compounds takes place at high temperatures [49]. Such compounds are present at the surface of the liquid film located at the top of the foam layer and exposed to the furnace atmosphere and to intense heating from the combustion space. They include alkali oxides, lead oxides, and boric oxides as well as sodium hydroxide (NaOH) or HCl in borosilicate glass [49, 71]. Their volatilization may significantly disturb concentration profiles in the liquid film and increase the liquid viscosity [49]. Then, the film surface becomes more rigid and even solid [49, 71]. However, the effect of volatilization on glass foam stability has received very little attention and is not accounted for in existing glass foam models.
4. In glass melting furnaces, the glass foam may be subjected to large temperature gradients but its effect on the foam dynamic behavior and stability remains to be explored and modeled. Bickford *et al.* [34] proposed an expression for the temperature gradient across the foam layer. The model accounted for heat generation due to chemical reactions and heat conduction. However, it did not account for radiative heat transfer within the foam where incident radiation from the furnace is scattered and absorbed [12, 13].
5. All the previously reviewed models used an average bubble radius. However, bubble size distribution can strongly affect the foam behavior. Thus, the model that explicitly accounts for the bubble size distribution rather than using the average bubble radius should be developed.

## 16.6 Measures for Reducing Glass Foaming in Glass Melting Furnaces

Destroying glass foam forming at the surface of glassmelt in industrial glass melting furnaces has been identified as one of the major issues in glass-melting technology [1]. The following sections make recommendations for reducing primary and secondary glass foaming based on the experimental observations and models previously described, as well as methods used in industry and described in patents. They consist of (i) facilitating the release of gases early in the melting process before a viscous liquid phase seals the batch, (ii) reducing the amount of gas generated, and/or (iii) destabilizing the liquid films separating the foam bubbles through various means.

### 16.6.1 Batch Composition

It has been established that secondary foaming can be reduced by facilitating the release of gases to the combustion space before the first liquid phase appears and becomes interconnected [74]. This can be achieved by adding carbonaceous compounds (e.g., coke, active carbon, graphite) to the batch. In particular, it can completely eliminate secondary foaming in high temperature regions of the furnace. However, it also tends to promote primary foaming due to early release of refining gases [55] and may change the oxidation state of the glass and its color. In addition, reducing conditions may attack metals, resulting in electric shorting between the electrode through the molten metal in electric melters [27].

Moreover, addition of  $\text{Na}_2\text{SO}_4$  to the batch reduces primary foaming in oxidized glasses [43, 74]. One should note that although  $\text{Na}_2\text{SO}_4$  reduces primary foaming, it also increases secondary foaming by enhancing refining reactions and gas production in the refining section. Therefore, the amount of  $\text{Na}_2\text{SO}_4$  to be added to the batch needs to be optimized by considering both primary and secondary foaming. Excessive reduction in the amount of refining agent may reduce glass fining and therefore result in reboil in the forehearth and reduced product quality. In furnaces equipped with oxygen-fuel burners the amount of refining agents added to the batch can be reduced compared with air-fuel burners. Here too, the batch content of refining agents needs to be optimized. Laimböck [43] proposed a semi-empirical expression for the optimal mass of sodium sulfate that should be added to the batch for producing soda-lime-silica glass with a given composition. It accounts for the maximum melting temperature, the water vapor partial pressure in the combustion space, the batch weight, the sulfate losses during initial fusion/melting reactions, and the small variations in the batch composition [43]. In particular,  $\text{SiO}_2$  and  $\text{Na}_2\text{O}$  contents should be carefully controlled as small variations ( $\sim 0.2$  wt%) may result in significant increase in the amount of refining gases released [43].

Alternatively, Pedebosq *et al.* [166] proposed adding sulfide to the batch as a way of reducing or eliminating secondary foaming in E-glass, alkali-resistant (AR) glass, C-glass, and S-glass featuring silica content less than 70 wt%. The sulfide can be added in the form of pure or mixed metal sulfide including  $\text{Na}_2\text{S}$ ,  $\text{CaS}$ ,  $\text{ZnS}$ ,  $\text{MOS}_2$ , and  $\text{CdS}$  as well as in the form of slag. It is also preferable to use sulfide particles smaller than  $200\mu\text{m}$  with concentration between 5 and 50 mol.% of refining agents  $\text{Na}_2\text{SO}_4$  or  $\text{CaSO}_4$ .

Furthermore, dissociating the oxidizing function of  $\text{Na}_2\text{SO}_4$  at low temperatures from its refining function at high temperature was proven to be successful at reducing glass foaming.

In fact, large amounts of  $\text{Na}_2\text{SO}_4$  could be replaced by oxidizing agents such as  $\text{NaBO}_3 \cdot \text{H}_2\text{O}$ ,  $\text{CaO}_2$ , and  $\text{NaNO}_3$  while maintaining the glass redox state. This proved to significantly reduce foaming in oxidized E-glass [46]. Similarly, Huang [7] proposed to add a high-temperature oxidizing agent to the batch such as cerium oxide and potassium permanganate. Such compounds are inactive at temperatures less than  $1315^\circ\text{C}$ , while they decompose and release oxygen gas above this temperature.

Finally, precise control of the glass redox state is important in controlling foaming. This is particularly challenging when recycled cullets, possibly contaminated, are mixed with the batch. Then, it is desirable to separate cullets by color and adjust the batch composition according to the type and amount of cullets used both to limit foaming and to achieve the desired glass redox state and color [43].

### 16.6.2 Batch Conditioning and Heating

Fine silica grains melt more quickly and create a viscous silica rich melt that traps the  $\text{CO}_2$  generated during primary foaming. Thus, using coarse silica grains and cullets favors the release of gases before the liquid phase is formed, thereby reducing primary foaming [113, 114]. However, more unmelted silica grains could remain in the final product. Alternatively, batch and cullets could be charged in the furnace in stratified layers with a moist batch layer consisting of coarse grains loaded on top of a layer of fine cullets [43]. This would not only enable the release of  $\text{CO}_2$  gas without being entrapped by a viscous melt but also accelerate the dissolution of silica sand [43].

Furthermore, compacting and preheating the batch and the cullets with the hot combustion products before introducing them into the furnace can significantly reduce foaming [72]. In particular, preheating the cullets enables the decomposition of organic contaminants in the form of  $\text{CO}_2$  and  $\text{CO}$ .

### 16.6.3 Furnace Temperature

On the one hand, increasing the furnace temperature tends to destabilize primary foaming [55, 70, 71] since the foam decay rate increases exponentially with temperature [71]. Note that directing the flames towards the batch logs to increase their temperature was not recommended as this may melt the top layer of the batch, thus preventing further gas release [43]. On the other hand, increasing temperature also shifts refining reactions towards gas production, which results in stronger secondary foaming. Thus, temperature increase should be accompanied by reduction in the content of refining agent. In addition, higher operating temperatures increase the fuel consumption, operating cost, and pollutant emissions, while reducing furnace lifetime. Moreover, slowly heating the batch was shown to reduce primary foaming [72, 74, 113–115], but it would also limit the plant productivity.

### 16.6.4 External and Temporary Actions

Numerous patents have been filed to control glass foams in industrial furnaces by using external means or temporary actions. The simplest way to destroy glass foams is to mechanically break the liquid films separating the bubbles. This can be achieved by using

mechanical rotators in the shape of a cone or a bar mounted on a rotating rod [67]. Alternatively, continuous or pulsating high pressure gas jets impinging onto the foams can be used [67, 167]. The gas jets may also carry large solid particles whose impact can mechanically break the liquid films [67]. During these processes, care should be taken not to affect the foam temperature and to choose gases that can be dissolved in the glassmelt as well as solid particles that do not contaminate the glass or generate gases.

Alternatively, Ito [168] proposed a method to eliminate foaming in molten slag by throwing a solid block containing (i) 17–72 wt% of organic material such as wood chips or powder as well as rice hulls, coal, tar, and pitch, (ii) 20–80 wt% of refractory materials such as silica, clay, olivine, limestone, dolomite, magnesite, and alumina, and (iii) 3–15 wt% of binder such as starch, sugars, and resins to hold the block together. The refractory ensured that the density of the block was heavier than the slag. Then, throwing the block caused significant mechanical disturbances, thus destroying the foam. In addition, the organic matter burns and decomposes at high temperatures, which destabilizes the foam. We speculate that the latter effect may be due to the fact that combustion of the organic matter consumes oxygen, producing a reducing atmosphere, known to destabilize liquid films, within the foam itself.

Moreover, Laimböck [43] proposed spraying  $\text{Na}_2\text{SO}_4$ , NaOH, and KOH solutions on the glass foam blanket as an efficient way to destroy it. Indeed, these elements significantly reduce surface tension of the glassmelt and induce a large surface tension gradient in the liquid films at the top of the foam, resulting in their destabilization.

More recently, Takei and Oda [169] patented a procedure to destroy glass foams by directly spraying inside the furnace metal oxide powders (e.g.,  $\text{TiO}_2$ ,  $\text{Al}_2\text{O}_3$ , ZnO) or solutions of organic metal compounds (e.g., tetramethyl silicate, metal tetrachloride, aluminum sulfate or nitrate) in water or organic solvents such as alcohols (e.g., ethanol) or hydrocarbons (hexane, toluene, kerosine). Metals of interest include Al, Ca, Ce, Co, Cr, Fe, Mg, Si, Ti, and Zn, which easily form metal oxide under oxidizing conditions and high temperatures. The metal compounds can be introduced by spraying particles or solutions in the air or oxygen flow used for combustion or through a separate carrier gas (e.g.,  $\text{N}_2$ ). They can also be mixed with heavy oil or natural gas before injection into the burner. They can also be mixed with water or organic solvents to form a slurry that can then be sprayed. As the metal compounds enter the furnace they oxidize and land on the glass foam preferably in the form of very fine metal oxide particles. The authors reported strong reduction in both foam coverage and energy consumption. The physical mechanism responsible is not clearly understood but it was suspected that these particles upon landing at the top of the glass foam disturb the liquid films by locally affecting the surface tension [169]. It could also be explained by the bridging–dewetting mechanism discussed in detail by Denkov and co-workers [86, 170].

Kappel *et al.* [71] observed that an increase in the pressure and pressure fluctuations of the furnace atmosphere favors decay of the foam. Harris [171] patented a method and apparatus to destroy foam in glass melting furnaces by directing pulses of compressed air or other gases towards the foam surface through pipes with or without nozzles. Alternatively, ultrasonic waves could be used to destroy glass foams [172]. These techniques have the advantage of not altering the glass composition. However, their practical implementation remains extremely challenging due to the large area of the glassmelt free surface and the high temperature and chemical conditions encountered in the combustion space.

Finally, Hammond *et al.* [173] proposed using a pulsed laser with emission wavelength corresponding to the absorption peak of the liquid phase. The laser produces local heating

of the foam, which destabilizes the liquid films. The laser beam can be shaped and scanned to cover a large surface area. The authors have successfully implemented this technique for aqueous foams but it could, in principle, be applied to glass foams.

### 16.6.5 Atmosphere Composition and Flame Luminosity

Sudden changes from oxidizing to reducing firing in the combustion space was found to be an effective way of destroying secondary foam in laboratory experiments [43, 55]. Direct implementation of this approach in industrial furnaces would require changing from an oxidizing to a reducing atmosphere in the entire combustion space. Indeed, partially implementing this method for some burners was not always successful as the changes at the foam surface need to be large enough to destabilize it [43]. Moreover, reducing atmosphere results in larger CO emission. Post-combustion of excess fuel may also cause excessive heating of the refractory walls, which reduces the furnace lifetime [43, 174]. Alternatively, Huang [7] proposed blowing an oxidizing gas such as oxygen, air, or steam onto the secondary foam to destroy it.

Rough [174] patented a method to prevent glass from foaming or to destabilize existing foams present at the surface of glassmelt by rapidly changing the oxygen concentration immediately above the glass foam. To do this, the author proposed repeatedly spraying oil, fuel gas, or finely divided carbonaceous materials such as carbon powder and cellulosic materials (e.g., wood, paper) directly on the glass foam. “Throwing wood” onto the foam was also described as a “conventional method” to destroy foams in molten slags [168]. These substances undergo rapid ignition and combustion, thus consuming the oxygen in the immediate vicinity of the glass foam. This action locally creates a reducing atmosphere, causing the glass foam to collapse as previously discussed [174]. The author also noticed that it was not necessary to change to composition of the entire combustion space to achieve the desired effects.

Finally, Barrow and Bird [80] proposed a method to destroy glass foam in industrial furnaces by directing a diffuse and luminescent flame towards the foam in the refining section or downstream region of the glass melting tank. Such a flame can be produced by injecting fuel (oil or natural gas) and oxidizer (air or oxygen) through two different ports or nozzles separated by a distance such that their mixing and combustion takes place far away from the injection ports. The fuel and oxygen ports should preferably be parallel and directed towards the glass melt surface. The authors reported partial or complete destruction of foams in flat glass furnaces using oxy-fuel firing. Note that the effect of the flame luminosity was also noticed in slag foaming [79]. The physical mechanism responsible for foam destruction was not completely understood but the authors speculated that soot particles made of carbon forming in diffuse luminescent flames might mechanically burst bubbles at the top of the foam [80]. Based on the phenomena reviewed in this chapter, other more likely mechanisms can be proposed, such as (i) temperature gradient along the foam surface, which destabilizes the liquid films, (ii) bridging and dewetting of the liquid thin films by the carbon particles [86,170], and (iii) local consumption of oxygen above the glass foam, which reacts with carbon, resulting in CO<sub>2</sub> production and a reducing atmosphere in a manner similar to that proposed by Rough [174].

### 16.6.6 Control Foaming in Reduced-pressure Refining

Several strategies have been proposed to control foaming in reduced-pressure refining. Note that many of them can be used in conventional furnaces under atmospheric pressure. First, Schwenninger *et al.* [175] proposed heating, by combustion, the headspace of the vacuum chamber in order to control foaming. Indeed, increasing the chamber temperature lowers the glassmelt viscosity and destabilizes the foam. In addition, the authors noted that the gases (e.g.,  $\text{CO}_2$  and  $\text{N}_2$ ) to be removed from the glassmelt should not be the products of the combustion reactions. Thus, they suggested burning carbon-free fuel, in particular  $\text{H}_2$ , with mainly  $\text{O}_2$ . The resulting water vapor dissolves in the melt and further lowers its viscosity and destabilizes the foam. Alternatively, they proposed the use of a plasma torch using carrier gases such as steam, hydrogen, oxygen, and inert gases. Note that combustion was sustained under reduced pressure and that no refining agents were needed for this refining process to be successful.

Moreover, Schwenninger *et al.* [176] suggested periodically applying short pulses of higher and/or lower pressure to control foaming during reduced-pressure refining. Alternatively, Pecoraro *et al.* [177] proposed adding large amounts of water (>0.05 wt%) to the glassmelt prior to entering the vacuum chamber. Then, water acts as a foaming agent and can serve as a substitute for a sulfate-refining agent with the advantage of being inexpensive and reducing equipment corrosion. In addition, water reduces both viscosity and surface tension. This results in larger bubbles that can easily escape the melt and accelerate foam decay. Water can be introduced to the melt by (i) melting the glassmelt in humid atmosphere, (ii) directly injecting steam within the glassmelt, or (iii) adding hydroxyl-rich batch components such as  $\text{NaOH}$  or  $\text{Na}_2\text{SiO}_3$ . Water also dilutes other gases present in the bubble and enhances refining as described in the so-called dilution model.

In addition, Welton *et al.* [178] suggested controlling foaming by spraying droplets of water and/or alkali metal (e.g.,  $\text{NaOH}$ ,  $\text{Na}_2\text{CO}_3$ ) solutions over the glass foam. In all cases, foam decay was attributed to several possible mechanisms responsible for destabilizing the liquid films separating the bubbles, including (i) mechanical breaking due to the impact of the droplet, (ii) thermal shock of the bubble lamellae, (iii) natural convection within the bubbles, and (iv) viscosity reduction caused by the increased water vapor or alkali contents of the melt. The authors also suggested the use of liquid fuel such as alcohol or fuel oil, whose combustion would increase the melt temperature, reduce its viscosity, and destabilize the foam. They also proposed injecting these liquids within the foam itself.

Finally, several methods have been developed to enhance foaming in reduced-pressure refining as a way to accelerate refining. In addition, rapid bubble expansion also accelerates the foam collapse by stretching the film separating bubbles [69]. The simplest method is to divide the stream of molten glass entering the vacuum chamber in smaller streams with possibly non-cylindrical shape in order to increase the surface area of glassmelt in contact with the low-pressure chamber [179]. Indeed, foaming is initiated near the surface of the glass stream and expands inside. Thus, reducing the thickness of the stream accelerates foaming and refining. A similar effect can be achieved by increasing the time during which the glass stream is in contact with the low pressure chamber [179]. In addition, Gerutti *et al.* [69] proposed adding very volatile selenium and/or tellurium to molten glass prior to entering the reduced-pressure chamber. Their premature volatilization can be minimized by adding oxidizing agents (e.g.,  $\text{NaNO}_3$ ) to the batch. The majority of the selenium can be

removed from the melt during the foaming process and thus does not affect significantly the glass composition and color. Finally, the use of other highly volatile substances featuring high vapor pressure has been proposed, including sulfates and halogens, also used as refining agents in conventional refining [180]. These enhanced foaming methods can be combined with the destruction methods previously reviewed to control excessive foaming.

## 16.7 Perspective and Future Research Directions

Despite advances in our understanding of glass foaming, numerous questions remain unanswered and further research is needed to be able to understand, predict, and control processes responsible for the formation of primary and secondary foams in industrial glass melting furnaces.

First, numerous defects and gas bubbles are produced during batch melting. Thus, it is essential to understand and model the retention of gas bubbles generated within the batch and their partitioning between the release to the combustion space and entrapment within the glassmelt. Such a model should account for the effects of (i) the batch grain and/or cullet size, (ii) the fusion/melting reactions, (iii) the heating rate, (iv) the refining reactions and gas generation, (v) the entrapment and escape of gases generated within the batch, (vi) the liquid flow and the liquid connectivity within the batch, (vii) changes in the effective thermal conductivity of the batch due to the appearance of entrapped gases, and (viii) the temperature gradients across the batch.

Moreover, several physical phenomena and foam characteristics are currently ignored in models predicting the transient and steady-state foam thickness of the foam layer. They include (i) the effects of bubble size distribution on glass foam stability, (ii) the temperature gradient across the foam layer, (iii) the fluctuations in the chemical composition, pressure, and temperature of the atmosphere surrounding the foam, (iv) the volatilization of volatile compounds and the resulting gradient in the local glass composition of the film, as well as (v) the possible chemical reactions and (vi) gas (e.g.,  $H_2O$ ) transport that may take place within the foams.

Furthermore, foam in glass melting furnaces may be generated in a specific area of the tank and spread over the glassmelt surface as it gets carried by surface convection currents or under its own weight and momentum. This increases the foam coverage of the glassmelt surface, which reduces its temperature. Therefore, experimental measurements and mathematical models for rheological properties of glass foams and their dependence on the foam morphology, chemical composition, and thermophysical properties are needed for predicting the spreading of the foam over the glassmelt free surface [152, 153].

In order to validate the physical models it would be highly desirable to develop a complete set of experimental data to verify the predictions of the theoretical models for glass foaming under controlled conditions representative of experimental and actual glass melting furnaces. Such a data set should contain complete characterization of (i) the batch (e.g., composition, grain size, compactness, porosity), (ii) the glassmelt composition, and (iii) glass foams (e.g., bubble size distribution and gas composition as well as porosity). The associated thermophysical properties of the glassmelt should also be available or measured. This is particularly true for the gas solubility, glassmelt viscosity,

and surface tension as a function of composition, temperature, and dissolved gas content. In addition, thermodynamics data are necessary to properly account for equilibrium redox reactions taking place at different stages and temperatures of the batch melting and foaming processes.

Finally, measurements of glass foams are made difficult by the fact that foams are metastable and by the thermal and chemical conditions present in glass melting furnaces. Experimentalists often have to rely on quenching the glass foams to “freeze” their state at a specific time during their formation [43, 46]. This is very difficult to perform without significantly affecting the sample and therefore can only provide partial information. Therefore, continuous and non-invasive diagnostic techniques able to monitor glass foams inside laboratory and industrial glass melting furnaces are highly desirable. Such techniques should be able to measure the thickness, porosity, gas composition, bubble size distribution, and temperature profile across the glass foam at high temperatures in both oxidizing and reducing atmospheres. These techniques, if available, would enable the investigation of highly temperature-dependent physical phenomena taking place in glass foams. They would also enable better real-time control of industrial furnaces and help us to understand phenomena that cannot be reproduced in laboratory experiments. For example, Solovjov *et al.* [181] proposed the use of diffusive-wave spectroscopy using steady-state and time-modulated laser beams to non-invasively determine thickness and optical properties of non-absorbing foams. Alternatively, Mengüç and co-workers [182–184] proposed the use of elliptically polarized light scattering to non-invasively determine the foam porosity and bubble size distribution.

## Acknowledgements

The author is indebted to Prof. Raymond Viskanta of Purdue University (West Lafayette, Indiana, USA) and Mr Rei Kitamura, Dr Shingo Urata and Mr Nagai of Asahi Glass Corporation (Yokohama, Japan) for kindly and thoroughly reviewing an earlier draft of this chapter.

## References

- [1] C.P. Ross and G.L. Tincher. *Glass Melting Technology: A Technical and Economic Assessment*. Glass Manufacturing Industry Council, Westerville, OH, 2004.
- [2] J.L. Barton. Present trends in industrial glass making. In *Proceedings of the XXI International Congress on Glass*, Beijing, China, vol. 1, October 9–14, 1995.
- [3] Barnes Reports. *2010 US Glass & Glass Product Manufacturing Industry Report*. NAICS 37721, C.Barnes & Co., March 2010.
- [4] H. G. Pfaender. *Schott Guide to Glass*. Chapman and Hall, London, 1996.
- [5] E. Worrell, C. Galitsky, E. Masanet and W. Graus. *Energy Efficiency Improvement and Cost Saving Opportunities for the Glass Industry*. Tech. Rep. LBNL-57335-Revision, Lawrence Berkeley National Laboratory, Berkeley, CA, 2008.
- [6] R. H. Doremus. *Glass Science*. John Wiley & Sons, New York, 1994.

- [7] J. Huang. Method for controlling secondary foam during glass melting. US patent no. 5,665,137, September 9, 1997.
- [8] J.E. Shelby. *Introduction to Glass Science and Technology*, 2nd edn. The Royal Society of Chemistry, Cambridge, 2005.
- [9] A.G. Fedorov and L. Pilon. Glass foam: formation, transport properties, and heat, mass, and radiation transfer. *J. Non-Crystalline Solids*, **311**(2): 154–73, 2002.
- [10] A. Ungan. Three dimensional numerical modeling of glass melting process. PhD thesis, Purdue University, West Lafayette, IN, 1985.
- [11] W. Trier, Wärmeübergang zwischen Flamme and Glasbad Glasschmelzwannenofen. *Glastechnische Berichte*, **36**(3): 73–86, 1963.
- [12] A.G. Fedorov and R. Viskanta. Radiative transfer in a semitransparent glass foam blanket. *Phys. Chem. Glasses*, **41**(3): 127–35, 2000.
- [13] A.G. Fedorov and R. Viskanta. Radiative characteristics of glass foams. *J. Am. Ceramic Soc.*, **83**(11): 2769–76, 2000.
- [14] L. Pilon and R. Viskanta. Radiation characteristics of glass containing gas bubbles. *J. Am. Ceramic Soc.*, **86**(8): 1313–20, 2003.
- [15] D. Baillis, L. Pilon, H. Randrianalisoa, R. Gomez and R. Viskanta. Measurements of radiation characteristics of fused-quartz containing bubbles. *J. Optical Soc. Am. A*, **21**(1): 149–59, 2004.
- [16] H. Randrianalisoa, D. Baillis and L. Pilon. Improved inverse method for determining radiation characteristics of fused quartz containing bubbles. *J. Thermophys. Heat Transfer*, **20**(4): 871–83, 2006.
- [17] L. Dombrovsky and D. Baillis. *Thermal Radiation in Disperse Systems: an Engineering Approach*. Begell House, New York, 1996.
- [18] J. Wang, B.S. Brewster, B.W. Webb and M.Q. McQuay. A numerical investigation on the thermal impact of foam on an oxy-fuel-fired glass furnace. *J. Energy Inst.*, **78**(3): 117–25, 2005.
- [19] F.W. Krämer. Properties of glass-forming melts. In *Properties of Glass-Forming Melts*, L.D. Pye, A. Montenero and I. Joseph (eds). Taylor & Francis, Boca Raton, FL, 2005.
- [20] Y. Kokubu, J. Chiba and T. Okamura. The behavior of sodium sulfate during glass melting process. In *Proceedings of the XI International Congress on Glass*, vol. 4, J. Götz (ed.). Prague, July 4–8, 1977.
- [21] D.W. Freitag and D.W. Richerson. Glass industry. In *Opportunities for Advanced Ceramics to Meet the Needs of the Industries of the Future*. Tech. Rep., US Department of Energy, 1998.
- [22] J. Stanek and J. Matej. Electric melting of glass. *J. Non-Crystalline Solids*, **84**(1–3): 353–62, 1986.
- [23] Y. Zhiqiang and Z. Zhihao. Basic flow pattern and its variation in different types of glass tank furnaces. *Glastechnische Berichte*, **70**: 165–72, 1997.
- [24] R. Viskanta, Review of three-dimensional mathematical modeling of glass melting, *J. Non-Crystalline Solids*, **177**: 347–62, 1994.
- [25] L. Pilon, *Interfacial and Transport Phenomena in Closed-Cell Foams*, PhD thesis, Purdue University, West Lafayette, IN, USA, 2002.
- [26] German Glass Societies HVG-DGG, View into a modern glass-melting tank, May 2010.
- [27] C.C. Chapman, J.M. Pope, and S.M. Barnes, Electric melting of nuclear waste glasses state of the art, *J. Non-Crystalline Solids*, **84**(1–3): 226–240, 1986.
- [28] A. Ungan and R. Viskanta. Effect of air bubbling on circulation and heat transfer in a glass-melting tank. *Journal of the American Ceramic Society*, **69**(5): 382–91, 1986.
- [29] B. Balkanlı and A. Ungan. Numerical simulation of bubble behaviour in glass melting tanks. Part 2. gas concentration. *Glass Technol.*, **37**(3): 101–5, 1996.
- [30] B. Balkanlı and A. Ungan. Numerical simulation of bubble behaviour in glass melting tanks. Part 3. bubble trajectories. *Glass Technol.*, **37**(4): 137–42, 1996.
- [31] L. Pilon, G. Zhao and R. Viskanta. Three-dimensional flow and thermal structures in glass melting furnaces. Part I. Effects of the heat flux distribution. *Glass Sci. Technol.*, **75**(2): 55–68, 2002.
- [32] D.S. Goldman, D.W. Brite and W.C. Richey. Investigation of foaming in liquid-fed melting of simulated nuclear waste glass. *J. Am. Ceramic Soc.*, **69**(5): 413–17, 1986.

- [33] D.S. Goldman. Melt foaming, foam stability and redox in nuclear waste vitrification. *J. Non-Crystalline Solids*, **84**(1–3): 292–8, 1986.
- [34] D.F. Bickford, P. Hrma, and B.W. Bowan. Control of radioactive waste glass melters: II, residence time and melt rate limitations. *J. Am. Ceramic Soc.*, **73**(10): 2903–15, 1990.
- [35] S.K. Bindal, A.D. Nikolov, D.T. Wasan, D.P. Lambert and D.C. Koopman. Foaming in simulated radioactive waste. *Environ. Sci. Technol.*, **35**(19): 3941–7, 2001.
- [36] M.I. Ojovan and W.E. Lee. Immobilisation of radioactive wastes in glass. In *An Introduction to Nuclear Waste Immobilisation*. Elsevier, Oxford, 2005.
- [37] C.F. De Voe. Electric glass melting furnace. US patent no. 2,490,339, December 6, 1949.
- [38] M. Williamson. Electric glass melting furnace. US patent no. 4,324,942, April 13, 1982.
- [39] P. Hrma. Model for a steady state foam blanket. *J. Coll. Interface Sci.*, **134**(1): 161–8, 1990.
- [40] D.K. Peeler, T.H. Lorier and J.D. Vienna. Melt rate improvement for DWPF MB3: Foaming theory and mitigation techniques. Tech. Rep. SR-1-6-WT-31, Pacific Northwest National Laboratory, Richland, WA, 2001.
- [41] P. Hrma. Melting of foaming batches: nuclear waste glass. In *Proceedings of the 2nd International Conference on Advances in the Fusion and Processing of Glass*, Düsseldorf, Germany, October 22–25, 1990.
- [42] F.W. Krämer. Solubility of gases in glass melts. *Berichte der Bunsengesellschaft für physikalische Chemie*, **100**(9): 1512–14, 1996.
- [43] P. R. Laimböck. Foaming of glass melts. PhD thesis, Technical University of Eindhoven, The Netherlands, 1998.
- [44] R.G.C. Beerkens and J. van der Schaaf. Gas release and foam formation during melting and fining of glass. *J. Am. Ceramic Soc.*, **89**(1): 24–35, 2006.
- [45] R.G.C. Beerkens. Sulphur chemistry and sulphate fining and foaming of glass melts, *Glass Technol.: Eur. J. Glass Sci. Technol. A*, **48**: 41–52, 2007.
- [46] A.J. Faber, O.S. Verheijen and J.M. Simon. Redox and foaming behavior of E-glass melts. In *Proceedings of the 7th International Conference on Advances in Fusion and Processing of Glass III, Rochester, NY vol. 141*, J.R. Varner, T.P. Seward III and H.A. Schaeffer (eds). The American Ceramic Society, July 27–31, 2003.
- [47] P.R. Laimböck and R.G.C. Beerkens. Oxygen sensor for float production lines. *Am. Ceramic Soc. Bull.*, **85**(5): 33–6, 2006.
- [48] C.R. Bamford. *Colour Generation and Control in Glass*. Elsevier Scientific Publishing Co., New York, 1977.
- [49] R.G.C. Beerkens. The role of gases in glass melting processes. *Glastechnische Berichte*, **71**(12): 369–80, 1995.
- [50] S. Kawachi and Y. Kawase. Evaluation of bubble removing performance in a TV glass furnace. Part 2. Verification using real furnace data. *Glastechnische Berichte*, **71**(5): 111–19, 1998.
- [51] E. Itoh, H. Yoshikawa, H. Miura and Y. Kawase. A quasi-stationary model for bubble behaviour in glass melts with refining reactions. *Glass Technol.*, **38**(4): 134–40, 1997.
- [52] S. Kawachi and Y. Kawase. Evaluation of bubble removing performance in a TV glass furnace. Part 1. Mathematical formulation. *Glastechnische Berichte*, **71**(4): 83–91, 1998.
- [53] M. Cable and A. A. Naqvi. The refining of a soda-lime-silica glass with antimony. *Glass Technol.*, **16**(1): 2–11, 1975.
- [54] L. Němec. Refining in the glassmelting process. *J. Am. Ceramic Soc.*, **60**(9/10): 436–40, 1977.
- [55] R.G.C. Beerkens and P. Laimböck. Foaming of glass melts. In *60th Conference on Glass Problems – Urbana, IL*, J. Kieffer (ed.). American Ceramic Society, October 19–20, 1999.
- [56] M. Cable and D. Martlew. The dissolution of silica in melts containing sodium carbonate, sodium sulphate, and silica. *Glass Technol.*, **37**(4): 137–42, 1996.
- [57] M. Arkosiová, J. Kloužek and L. Němec. The role of sulfur in glass melting processes. *Ceramics–Silikáty*, **52**(3): 155–9, 2008.
- [58] P. Hrma, Effect of heating rate on glass foaming: transition to bulk foam. *J. Non-Crystalline Solids*, **355**(4/5): 257–63, 2009.
- [59] R.G.C. Beerkens and H. De Wall. Mechanism of oxygen diffusion in glassmelts containing variable-valence ions. *J. Am. Ceramic Soc.*, **73**(7): 1857–61, 1990.

- [60] R. Pyare, S. P. Singh, A. Singh and P. Nath. The  $As^{3+}$ - $As^{5+}$  equilibrium in borate and silicate glasses. *Phys. Chem. Glasses*, **23**(5): 158–68, 1982.
- [61] S. Kawachi and M. Kato. Evaluation of reaction rate of refining agents. *Glastechnische Berichte*, **72**(6): 182–7, 1999.
- [62] L. Némec. The behaviour of bubbles in glass melts. Part 1. Bubble size controlled by diffusion. *Glass Technol.*, **21**(3): 134–8, 1980.
- [63] J.-T. Olink. Apparatus for melting and refining glass. US patent no. 3,519,412, July 7, 1970.
- [64] G.E. Kunkle, W.M. Welton and R.L. Schwenninger. Melting and vacuum refining of glass or the like and composition of sheet. US patent no. 4,738,938, April 19, 1988.
- [65] S. Takeshita, C. Tanaka and K. Ishimura. Refining method for molten glass and an apparatus for refining molten glass. US patent no. 5,849,058, December 15, 1998.
- [66] T. Kawaguchi, K. Obayashi, M. Okada, and Y. Takei. Vacuum degassing method for molten glass flow. US patent no. 6,332,339, December 25, 2001.
- [67] J.C. Hayes, R.A. Murnane, R.W. Palmquist and F. Woolley. Method for controlling foam production in reduced pressure fining. US patent no. 6,854,290 B2, February 15, 2005.
- [68] J.C. Hayes. Method for controlling foam production in reduced pressure fining. US patent no. 7,134,300 B2, November 14, 2006.
- [69] R.L. Gerutti, D.R. Haskins, R.B. Heithoff, R.L. Schwenninger and W.M. Welton. Method of vacuum refining of glassy materials with selenium foaming agent. US patent no. 4,886,539, December 12, 1989.
- [70] A. Gerrard and I.H. Smith. Laboratory techniques for studying foam formation and stability in glass melting. In *Glastechnische Berichte XIII. Internationaler Glaskongress*, vol. 56K, July 4–9 1983.
- [71] J. Kappel, R. Conradt and H. Scholze. Foaming behavior on glass melts. *Glastechnische Berichte*, **60**(6): 189–201, 1987.
- [72] J.S. Ahn and P. Hrma. Effect of heat pretreatment on foaming of simulated nuclear waste in a borosilicate glass melt. *Adv. Ceramics*, **20**: 181–90, 1986.
- [73] G.A. Pecoraro. How the properties of glass melts influence the dissolution of refractory materials. In *Properties of Glass-Forming Melts*, L.D. Pye, A. Montenero and I. Joseph (eds). Taylor & Francis, Boca Raton, FL, pp. 337–389, 2005.
- [74] D.-S. Kim and P.R. Hrma. Volume changes during batch to glass conversion. *Am. Ceramic Soc. Bull.*, **69**(6): 1039–43, 1990.
- [75] M. Cable, C.G. Rasul and J. Savage. Laboratory investigation of foaming and reboil in soda-lime-silicate melts. *Glass Technol.*, **9**(2): 25–31, 1968.
- [76] S.M. Budd, V.H. Exelby and J.J. Kirwan. The formation of gas bubbles in glass at high temperature. *Glass Technol.*, **3**(4): 124–9, 1962.
- [77] C.G. Rasul and M. Cable. Spontaneous bubble formation in silicate melts at high temperatures. *J. Am. Ceramic Soc.*, **49**(10): 568–71, 1966.
- [78] M. Cable and C.G. Rasul. Spontaneous bubble formation in silicate melts at high temperatures. II: Effect of wet atmospheres and behavior of mixed alkali glasses, *J. Am. Ceramic Soc.*, **50**(10): 528–31, 1967.
- [79] C. F. Cooper and J.A. Kitchener. The foaming of molten silicates. *J. Iron and Steel Inst.*, 48–55, 1959.
- [80] T. Barrow and D.A. Bird. Melting of glass. US patent no. 6,715,319, April 6, 2004.
- [81] G. Narsimhan and E. Ruckenstein. Effect of bubble size distribution on the enrichment and collapse in foams. *Langmuir*, **2**: 494–508, 1986.
- [82] A. Bhakta and E. Ruckenstein. Decay of standing foams: drainage, coalescence and collapse. *Adv. Coll. Interface Sci.*, **70**: 1–124, 1997.
- [83] F. Geotti-Bianchini, J.T. Brown, A.J. Faber, H. Hessenkemper, S. Kobayashi and I.H. Smith. Influence of water dissolved in the structure of soda-lime-silicate glass on melting, forming and properties: state-of-the-art and controversial issues. *Glastechnische Berichte*, **72**(5): 145–52, 1999.
- [84] K.-H. Hess and D.D. Dingwell. Viscosities of hydrous leucogranitic melts: a non-Arrhenian model. *Am. Mineralogist*, **81**: 1297–300, 1996.

- [85] K. Zähringer, J.-P. Martin, and J.P. Petit. Numerical simulation of bubble growth in expanding perlite. *J. Mater. Sci.*, **36**: 2691–705, 2001.
- [86] J.T. Petkov and N.D. Denkov. Dynamics of particles on interfaces and in thin liquid films. In *Encyclopedia of Surface and Colloid Science*, 2nd edn, P. Somasundaran and A. Hubbard (eds). Taylor and Francis, New York, 2006.
- [87] A. Kucuk, A.G. Clare, and L. Jones. An estimation of the surface tension of silicate glass melts at 1400°C using statistical analysis. *Glass Technol.*, **40**(5): 149–53, 1999.
- [88] N. P. Bansal and R.H. Doremus. *Handbook of Glass Properties*. Academic Press, San Diego, CA, 1986.
- [89] J. Kappel and H. Roggendorf. Origin, stability, and decay of foam on glass melts. In *Proceedings of the 2nd International Conference on Advances in the Fusion and Processing of Glass*, Düsseldorf, October 22–5, 1990.
- [90] N. M. Parikh. Effect of atmosphere on surface tension of glass. *J. Am. Ceramic Soc.*, **41**: 18–22, 1958.
- [91] O. T. Roi, G. Nölle Seidel and D. Höhne. Formation and behavior of bubble curtains in glass melts. *Glastechnische Berichte*, **68**(7): 222–7, 1995.
- [92] G. Debrégeas, P.-G. de Gennes and F. Brochard-Wyart. The life and death of bare viscous bubbles. *Science*, **279**: 1704–7, 1998.
- [93] R.B. Jucha, D. Powers, T. McNeil, R.S. Subramanian and R. Cole. Bubble rise in glassmelts. *J. Am. Ceramic Soc.*, **65**(6): 289–92, 1982.
- [94] J.E. Shelby. *Handbook of Gas Diffusion in Solids and Melts*. ASM International, Materials Park, OH, 1996.
- [95] E.M. Hornyak and M.C. Weinberg. Velocity of a freely rising gas bubble in a soda-lime silicate glass melt. *Comm. Am. Ceramic Soc.*, **67**(11): C244–6, 1984.
- [96] L. Němec. Diffusion-controlled dissolving of water vapor bubbles in molten glass. *Glass Technol.*, **10**: 176–81, 1969.
- [97] M.C. Weinberg, P.I.K. Onorato and D.R. Uhlmann. Behavior of bubbles in glass-melts: I, dissolution of a stationary bubble containing a single gas. *J. Am. Ceramic Soc.*, **63**: 175–80, 1980.
- [98] H. Yoshikawa and Y. Kawase. Significance of redox reactions in glass refining processes. *Glastechnische Berichte*, **70**(2): 31–40, 1997.
- [99] M. Cable and J.R. Frade. Theoretical analysis of the dissolution of multi-component gas bubbles. *Glastechnische Berichte*, **60**(11): 355–62, 1987.
- [100] M.C. Weinberg, P.I.K. Onorato and D.R. Uhlmann. Behavior of bubbles in glassmelts: II, dissolution of a stationary bubble containing a diffusing and a non-diffusing gas. *J. Am. Ceramic Soc.*, **63**: 435–8, 1980.
- [101] P.I.K. Onorato, M.C. Weinberg and D.R. Uhlmann. Behavior of bubbles in glassmelts: III, dissolution and growth of a rising bubble containing a diffusing a single gas. *J. Am. Ceramic Soc.*, **64**: 676–82, 1981.
- [102] B. Balkanli and A. Ungan. Numerical simulation of bubble behaviour in glass melting tanks. Part 1. under ideal conditions. *Glass Technol.*, **37**(1): 29–34, 1996.
- [103] E. Itoh, H. Yoshikawa, and Y. Kawase. Modeling of bubble removal from glassmelts at fining temperatures. *Glastechnische Berichte*, **70**(1): 8–16, 1997.
- [104] J.I. Ramos. Behavior of multicomponent gas bubbles in glass melts. *J. Am. Ceramic Soc.*, **69**(2): 149–54, 1986.
- [105] H. Yoshikawa, H. Miura and Y. Kawase. Dissolution of bubbles in glassmelts with equilibrium redox reactions: approximations for a moving bubble boundary. *J. Mater. Sci.*, **33**(10): 2701–7, 1998.
- [106] A. Ungan, W.H. Turner and R. Viskanta. Effect of gas bubbles on three-dimensional circulation in a glass melting tank. *Glastechnische Berichte*, **56K**: 125–9, 1983.
- [107] D. Ramkrishna. *Population Balances: Theory and Applications to Particulate Systems in Engineering*. Academic Press, San Diego, CA, 2000.
- [108] O. T. Roi, G. Nölle Seidel and D. Höhne. Modeling of bubble population in glass melts. *Glastechnische Berichte*, **67**(10): 263–71, 1994.
- [109] B. Balkanli and A. Ungan. Numerical simulation of bubble behaviour in glass melting tanks. Part 4: Bubble number density distribution. *Glass Technol.*, **3**(5): 164–8, 1996.

- [110] L. Pilon, A.G. Fedorov, D. Ramkrishna and R. Viskanta. Bubble transport and generation in glass melting furnaces. part I. mathematical formulation. *J. Non-Crystalline Solids*, **336**(2): 71–83, 2004.
- [111] L. Pilon and R. Viskanta. Bubble transport and generation in glass melting furnaces. Part II: Numerical results. *J. Non-Crystalline Solids*, **336**(2): 84–95, 2004.
- [112] S.L. Chang, C.Q. Zhou and B. Golchert. Eulerian approach for multiphase flow simulation in a glass melter. *Appl. Thermal Eng.*, **25**(17/18): 3083–103, 2005.
- [113] D.-S. Kim and P.R. Hrma. Foaming in glass melts produced by sodium sulfate decomposition under isothermal conditions. *J. Am. Ceramic Soc.*, **74**(3): 551–5, 1991.
- [114] D.-S. Kim and P.R. Hrma. Foaming in glass melts produced by sodium sulfate decomposition under ramp heating conditions. *J. Am. Ceramic Soc.*, **75**(11): 2959–63, 1992.
- [115] D.-S. Kim, B.C. Dutton, P.R. Hrma and L. Pilon. Effect of furnace atmosphere on E-glass foaming. *J. Non-Crystalline Solids*, **352**(50/51): 5287–95, 2006.
- [116] M. Arkosiová, J. Kloužek and L. Němec. Sulfur functioning during glass melting. *Advanced Materials Research*, **39/40**: 413–18, 2008.
- [117] J. van der Schaaf and R.G.C. Beerkens. A model for foam formation, stability, and breakdown in glass-melting furnaces. *J. Coll. Interface Sci.*, **295**(1): 218–29, 2006.
- [118] D.-S. Kim, M. Portch, J. Matyas, P.R. Hrma and L. Pilon. *Foaming of E-Glass II*. Tech. Rep. PNNL-15394, Pacific Northwest National Laboratory, Richland, WA, 2005.
- [119] G. Bayer. Foaming of borosilicate glasses by chemical reactions in the temperature range 950–1150°C. *J. Non-Crystalline Solids*, **38/39**(2): 855–60, 1980.
- [120] E. Bernardo and F. Albertini. Glass foams from dismantled cathode ray tubes. *Ceramics Int.*, **32**: 603–8, 2006.
- [121] E. Bernardo, R. Cedro, M. Florean and S. Hreglich. Reutilization and stabilization of wastes by the production of glass foams. *Ceramics Int.*, **33**(6): 963–8, 2007.
- [122] E. Bernardo. Micro- and macro-cellular sintered glass-ceramics from wastes. *J. Eur. Ceramic Soc.*, **27**(6): 2415–22, 2007.
- [123] E. Bernardo, G. Scarinci, P. Bertuzzi, P. Ercole and L. Ramon. Recycling of waste glasses into partially crystallized glass foams. *J. Porous Mater.*, **17**(3): 359–65, 2010.
- [124] F. Méar, P. Yot, M. Cambon and M. Ribes. Elaboration and characterisation of foam glass from cathode ray tubes. *Adv. Appl. Ceramics*, **104**: 123–30, 2005.
- [125] F. Méar, P. Yot, M. Cambon and M. Ribes. The changes in lead silicate glasses induced by the addition of a reducing agent (tin or sic). *J. Non-Crystalline Solids*, **351**(40–2): 3314–19, 2005.
- [126] F. Méar, P. Yot and M. Ribes. Effects of temperature, reaction time and reducing agent content on the synthesis of macroporous foam glasses from waste funnel glasses. *Mater. Lett.*, **60**(7): 929–34, 2006.
- [127] F. Méar, P. Yot, M. Cambon and M. Ribes. The characterization of waste cathode-ray tube glass. *Waste Management*, **26**(12): 1468–76, 2006.
- [128] F. Méar, P. Yot, M. Cambon, R. Caplain and M. Ribes. Characterisation of porous glasses prepared from cathode ray tube (CRT). *Powder Technol.*, **162**(1): 59–63, 2006.
- [129] F. Méar, P. Yot, R. Viennois and M. Ribes. Mechanical behaviour and thermal and electrical properties of foam glass. *Ceramics Int.*, **33**(4): 543–50, 2007.
- [130] S. Herat. Recycling of cathode ray tubes (CRTs) in electronic waste. *CLEAN: Soil, Air, Water*, **36**(1): 19–24, 2008.
- [131] D. Lv, X. Li, L. Wang, J. Du and J. Zhang. Effect of carbon as foaming agent on pore structure of foam glass. *Adv. Mater. Res.*, **105/106**: 765–8, 2010.
- [132] R.G.C. Beerkens, L. Zaman, P. Laimböck and S. Kobayashi. Impact of furnace atmosphere and organic contamination of recycled cullet on redox state and fining of glass melts. *Glastechnische Berichte*, **72**(5): 127–44, 1999.
- [133] K. Papadopoulos. The solubility of SO<sub>3</sub> in soda-lime-silica melts. *Phys. Chem. Glasses*, **14**(3): 60–5, 1973.
- [134] C.J.B. Fincham and F.D. Richardson. The behaviour of sulphur in silicate and aluminat melts. *Proc. R. Soc. Lond. A*, **223**(1152): 40–62, 1954.
- [135] F. Geotti-Bianchini and L. De Riu. Water content of sulfate-fined industrial soda-lime glass and its influence on workability. *Glastechnische Berichte*, **71**(8): 230–42, 1998.

- [136] P.B. McGinnis and J.E. Shelby. Diffusion of water in float glass melts. *J. Non-Crystalline Solids*, **177**: 381–8, 1994.
- [137] J.J. Bikerman. The unit of foaminess. *Trans. Faraday Soc.*, **38**: 634–8, 1938.
- [138] S.A.K. Jeelani, S. Ramaswami and S. Hartland. Effect of binary coalescence on steady-state height of semi-batch foams. *Chem. Eng. Res. Des.*, **68**(3): 271–7, 1990.
- [139] S. Hartland, J.R. Bourne and S. Ramaswami. A study of disproportionation effects in semi-batch foams. II: Comparison between experiment and theory. *Chem. Eng. Sci.*, **48**: 1723–33, 1993.
- [140] S.S. Ghag, P.C. Hayes and H.-G. Lee. Physical model studies on slag foaming. *ISIJ Int.*, **38**: 1201–7, 1998.
- [141] D.B. Buruk, D. Petrovic and J.G. Daly. Flow regime transitions in a bubble column with a paraffin wax as the liquid medium. *Ind. Eng. Chem. Res.*, **26**: 1087–92, 1987.
- [142] L.Z. Pino, M.M. Yopez, A.E. Saez and G. De Drago. An experimental study of gas holdup in two-phase bubble columns with foaming liquids. *Chem. Eng. Comm.*, **89**: 155–75, 1990.
- [143] Y.T. Shah, S. Joseph, D.N. Smith and J.A. Ruether. On the behavior of the gas phase in a bubble column with ethanol–water mixtures. *Ind. Eng. Chem. Process Des. Dev.*, **24**: 1140–8, 1985.
- [144] K. Ito and R.J. Fruehan. Study of the foaming of CaO-SiO<sub>2</sub>-FeO slags. Part I: Foaming parameters and experimental results. *Metall. Mater. Trans. B*, **20B**: 509–14, 1989.
- [145] K. Ito and R.J. Fruehan. Study of the foaming of CaO-SiO<sub>2</sub>-FeO slags. Part II: Dimensional analysis and foaming in iron and steelmaking processes. *Metall. Mater. Trans. B*, **20B**: 515–21, 1989.
- [146] R. Jiang and R.J. Fruehan. Slag foaming in bath smelting. *Metall. Mater. Trans. B*, **22B**: 481–9, 1991.
- [147] Y. Zhang and R.J. Fruehan. Effect of bubble size and chemical reactions on slag foaming. *Metall. Mater. Trans. B*, **26B**: 803–12, 1995.
- [148] Y. Zhang and R.J. Fruehan. Effect of gas type and pressure on slag foaming. *Metall. Mater. Trans. B*, **26B**: 1089–91, 1995.
- [149] B. Ozturk and R.J. Fruehan. Effect of temperature on slag foaming. *Metall. Mater. Trans. B*, **26B**: 1086–8, 1995.
- [150] S.-M. Jung and R.J. Fruehan. Foaming characteristics of BOF slags. *ISIJ Int.*, **40**: 348–54, 2000.
- [151] R.C. Watkins. An improved foam test for lubricating oils. *J. Inst. Petrol.*, 106–13, 1973.
- [152] B.Y. Lattimer and J. Trelles. Foam spread over a liquid pool. *Fire Safety J.*, **42**(4): 249–64, 2007.
- [153] B. Persson, A. Lönnermark and H. Persson. Foamsplex: large scale foam application-modelling of foam spread and extinguishment. *Fire Technol.*, **39**: 347–62, 2003.
- [154] L. Pilon, A.G. Fedorov and R. Viskanta. Analysis of transient thickness of pneumatic foams. *Chem. Eng. Sci.*, **57**: 977–90, 2002.
- [155] L. Pilon, A.G. Fedorov and R. Viskanta. Steady-state foam thickness of liquid–gas foams. *J. Coll. Interface Sci.*, **242**: 425–36, 2001.
- [156] L.L. Schramm. *Dictionary of Colloid and Interface Science*. Wiley and Sons, New York, 2001.
- [157] R. McElroy. Air release from mineral oils. PhD thesis, Department of Pure and Applied Chemistry, Strathclyde University, 1978.
- [158] Z. Lin and R.I.L. Guthrie. A model for slag foaming for the in-bath smelting process. *Iron and Steelmaker*, **22**(5): 67–73, 1995.
- [159] L. Pilon and R. Viskanta. Superficial gas velocity for onset of foaming. *Chem. Eng. Process.*, **43**(2): 149–60, 2004.
- [160] G.B. Wallis. *One-Dimensional Two-Phase Flow*. McGraw-Hill, New York, 1969.
- [161] Y. Zhang and R.J. Fruehan. Effect of carbonaceous particles on slag foaming. *Metall. Mater. Trans. B*, **26B**: 813–19, 1995.
- [162] S.S. Ghag, P.C. Hayes and H.-G. Lee. Model development of slag foaming. *ISIJ Int.*, **38**: 1208–15, 1998.
- [163] S.S. Ghag, P.C. Hayes and H.-G. Lee. The prediction of gas residence times in foaming CaO-SiO<sub>2</sub>-FeO. *ISIJ Int.*, **38**: 1216–24, 1998.

- [164] D. Lotun and L. Pilon. Physical modeling of slag foaming for various operating conditions and slag compositions. *ISIJ Int.*, **45**(6): 835–40, 2005.
- [165] G. Narsimhan. A model for unsteady state drainage of a static foam. *J. Food Eng.*, **14**: 139–65, 1991.
- [166] P. Pedebosq, R. Jacques and A. Berthereau. Glass melting in the presence of sulfur. US patent application publication no. US 2009/0277227 A1, November 12, 2009.
- [167] W.H. Echols. Apparatus for breaking up a foam. US patent no. 3,298,615, January 17, 1964.
- [168] H. Ito. Method for defoaming molten slag. US patent no. 4,042,410, August 16, 1977.
- [169] Y. Takei and K. Oda. Method for melting glass. US patent no. 6,470,710 B1, October 29, 2002.
- [170] N.D. Denkov and K.G. Marinova. Antifoam effects of solid particles, oil drops and oil-solid compounds in aqueous foams. In *Colloidal Particles at Liquid Interfaces*, B.P. Binks and T.S. Horozov (eds). Cambridge University Press, Cambridge, 2006.
- [171] J.L. Harris. Apparatus for dissipating foam on molten glass. US patent no. 3,649,235, March 14, 1972.
- [172] S.V. Komarov, M. Kuwabara and M. Sano. Control of foam height by using sound waves. *ISIJ Int.*, **39**(12): 1207–16, 1999.
- [173] P. Hammond. Foam control. US patent no. 6,599,948 B1, July 29, 2003.
- [174] R.R. Rough. Method of eliminating a foam blanket on the surface of molten glass. US patent no. 3,350,185, October 31, 1967.
- [175] R.L. Schwenninger and J.M. Matesa. Vacuum refining of glassy materials with controlled foaming. US patent no. 4,704,153, November 3, 1987.
- [176] R.L. Schwenninger, D.A. Hanekamp, and H.R. Foster. Pulsed pressure method for vacuum refining of glassy materials. US patent no. 4,849,004, July 18, 1989.
- [177] G.A. Pecoraro, L.J. Shelestak and J.E. Cooper. Vacuum refining of glassy materials with selected water content. US patent no. 4,919,700, April 24, 1990.
- [178] W.M. Welton. Foam control method for vacuum refining of glassy materials. US patent no. 4,794,860, January 3, 1989.
- [179] R.L. Schwenninger, W.M. Welton, B.S. Dawson, J.M. Matesa and L.J. Shelestak. Vacuum refining of glass or the like with enhanced foaming. US patent no. 4,780,122, October 25, 1988.
- [180] G.A. Pecoraro, L.J. Shelestak and J.E. Cooper. Vacuum refining of glassy materials with selected foaming rate. US patent no. 4,919,697, April 24, 1990.
- [181] V.P. Solovjov, M.R. Jones, K.E. Fackrell and B.W. Webb. Characterization of industrial foams. In *Proceedings of the ASME International Mechanical Engineering Congress*, New Orleans, November 17–22, 2002, IMECE 2002–33905.
- [182] B.T. Wong and M.P. Mengüç. Depolarization of radiation by non-absorbing foams. *J. Quant. Spectroscopy Radiative Transfer*, **73**(2–5): 273–84, 2002.
- [183] J.N. Swamy, C. Crofcheck and M.P. Mengüç. A Monte Carlo ray tracing study of polarized light propagation in liquid foams. *J. Quant. Spectroscopy Radiative Transfer*, **104**(2): 277–87, 2007.
- [184] J.N. Swamy, C. Crofcheck and M.P. Mengüç. Time dependent scattering properties of slow decaying liquid foams. *Coll. Surf. A: Physicochem. Eng. Aspects*, **338**(1–3): 80–6, 2009.